DOPPLER SODAR OBSERVATIONS OF THE WINDS AND STRUCTURE IN THE LOWER ATMOSPHERE OVER FAIRBANKS, ALASKA

By

Pavan Kumar Reddy Kankanala

RECOMMENDED: _____

_____

_____

_____
Advisory Committee Chair

_____
Chair, Atmospheric Sciences Program

APPROVED: _____
Dean, College of Natural Science and Mathematics

_____
Dean of the Graduate School

_____
Date

DOPPLER SODAR OBSERVATIONS OF THE WINDS AND STRUCTURE IN THE LOWER ATMOSPHERE OVER FAIRBANKS, ALASKA

A

THESIS

Presented to the Faculty

of the University of Alaska Fairbanks

in Partial Fulfillment of the Requirements

for the Degree of

MASTER OF SCIENCE

By

Pavan Kumar Reddy Kankanala, B.Tech.

Fairbanks, Alaska

December 2007

Abstract

Fairbanks, Alaska (64^0 49′ N, 147^0 52′ W) experiences strong temperature inversions which when combined with the low wind speeds prevailing during the winter cause serious air pollution problems. The SODAR (Sound Detection And Ranging) or acoustic sounder is a very useful instrument for studying the lower atmosphere as it can continuously and reliably measure the vertical profiles of wind speed and direction, vertical motions, turbulence and the thermal structure in the lower part of the troposphere. A Doppler sodar was operated from December 2005 to April 2006 at the National Weather Service site in Fairbanks. The wind observations from the sodar indicate that the majority of the winds during the winter months were from the North, Northeast or the East, which is in good agreement with the radiosonde measurements and the long term trends in the wind patterns over Fairbanks area. Case studies were carried out using the sodar data depicting drainage winds, low-level jets, formation and breakup of inversions and estimation of the mixing layer height.

Table of Contents

Page

Page

List of Figures

Page

Page

Acknowledgments

I would like to take this opportunity to thank a variety of people whose help has been instrumental in accomplishing this task.

First I would like to thank my advisor Dr. Kenneth Sassen for providing me an opportunity to work on this project. I gratefully acknowledge the valuable guidance and support he provided. I thank my advisory committee members Dr. David Atkinson, Dr. Richard Collins and Dr. Glenn Shaw for their valuable input in this work. I thank Dr. Javier Fochesatto for his valuable comments and suggestions and the motivational support that he provided. I also want to acknowledge the National Weather Service for providing the site location and facilities to operate the equipment. The machine shop of the Geophysical Institute assisted me in the transportation, installation and maintenance of the equipment. Thanks for the great job in the freezing cold.

I would also like to thank the faculty of the atmospheric sciences program here at the UAF for their help in comprehending the required coursework, providing with the background knowledge and in my overall development. I thank my fellow students in the atmospheric sciences program especially Dr. James Campbell, Patrick Cobb, Debasish Pai Mazumder and Ramaswamy Tiruchirapalli for their continued support and creating a pleasant environment to learn.

I am grateful to my friends and family members for their encouragement and support throughout my life.

This research work was supported by UPOS and NASA grants NNG04GF35G.

Chapter 1 Introduction

The surface-based temperature inversion is a frequently occurring feature of the high-latitude climate. A temperature inversion is defined as an increase of air temperature with altitude, which is opposite to the usual decrease of temperature with height, in the troposphere. Inversions are created by radiative cooling of lower layers close to the surface, by subsidence heating of an upper layer, or by advection of warm air over cooler air or of cool air under warmer air. A surface-based inversion layer is primarily driven by a deficit of solar radiation at the Earth's surface. This low-level inversion can become strong, inhibiting the mixing of surface-level air with that of the overlying free troposphere and thus playing an important role in the dynamics of the Arctic planetary boundary layer (Kahl, 1990).

Fairbanks, (64^0 49′ N, 147^0 52′ W), the second largest city in the state of Alaska, lies in the interior of Alaska between the climatic divides of the Brooks Range to the north and Alaska Range to the south. It is situated on the northern edge of the broad, flat valley of the Chena-Tanana River Basins. Figure 1.1 shows the topographic setting of Fairbanks. The city is surrounded by a rough semicircle of hills rising 300 to 600m extending from northeast to southwest and 50km to the south the foot hills of the Alaska Range forms another barrier. Due to the high latitude, local topography and the distance from the sea, the winter time temperature inversions in Fairbanks are among the strongest in the world (Bilello, 1966; Benson and Weller, 1969; Wendler, 1969).

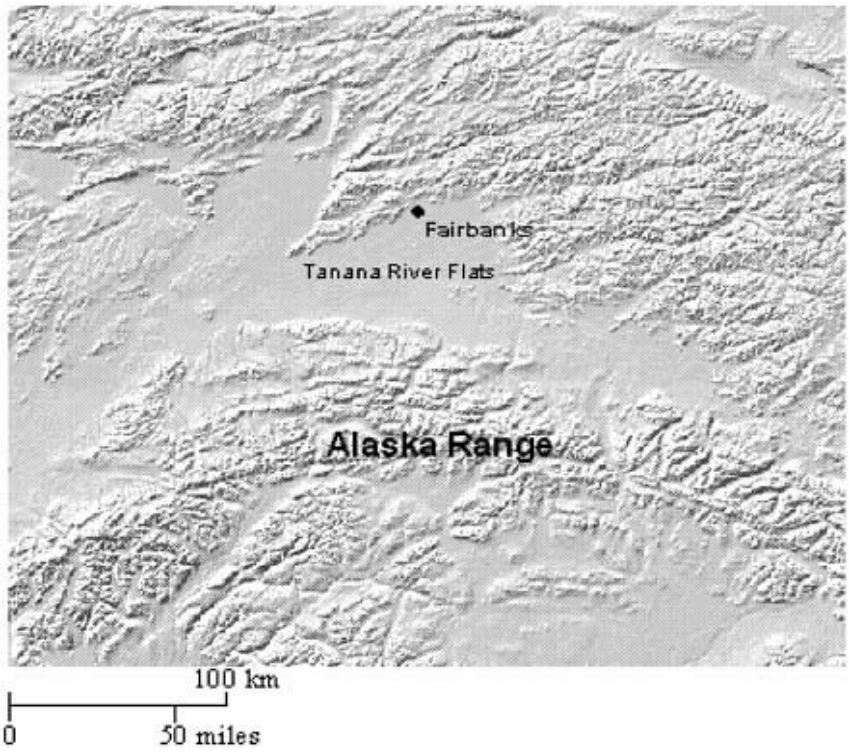

Figure 1.1 Topographic map of the Fairbanks area. (Source: The Ongoing Challenge of Managing Carbon Monoxide Pollution in Fairbanks, Alaska; Committee on Carbon Monoxide Episodes in Meteorological and Topographical Problem Areas, National Research Council, 2002).

1.1 Climatic features in Fairbanks during winter

1.1.1 Temperature inversions

The continental climate of Fairbanks exhibits a typical continental-type climate, defined by large swings between a January mean temperature of around -25°C and a July mean of about 15°C. Summer temperatures can frequently reach 30°C and have exceeded 35°C on occasion, and winter temperatures may dip as low as -50°C (Benson et al., 1983). These low temperatures are a result of the steep ground inversions, primarily driven by a deficit of solar radiation, which can be maintained due to the low surface

wind speeds in Fairbanks owing to its sheltered location. Bowling et al. (1968) show a strong connection between the occurrence of lowest temperatures in Fairbanks with high pressure systems and clear skies. A sharp temperature drop at the surface is correlated with the decrease of cloudiness and at these times the surface inversion is built up. On the other hand with the onset of cloudiness the surface temperature increases and reaches a maximum determined by the temperature of the cloud. By analyzing 9 years of radiosonde data for Fairbanks, Bilello (1966) found that the frequency of surface inversions for both day and night is highest at 82% in the coldest months (December-January), averages 68% for the other winter months (November-April), and 37% for the summer (May-October).

During these situations of extreme ground inversions and low wind speeds a turbulent mixing layer, characterized by well-developed turbulence and approximately height-independent fluxes of heat and momentum, is generally missing at the surface. As a result surface pollutants such as combustion products and ice fog, when the temperature decreases below about -30°C (Benson, 1970), are trapped within a few hundred feet above the ground causing serious air pollution problems.

1.1.2 Valley winds and drainage winds

During winter, wind speeds in Fairbanks are very low and both speed and direction are density driven and thus strongly controlled by topography with stronger winds generated on steep slopes and weaker winds on relatively flat terrain. The surface wind speed during situations of strong inversions is generally less than $0.5 ms^{-1}$, as contrasted

with the frequent value for all seasons being 0.4 to 0.9ms^{-1}, and the main flow direction within the Boundary Layer (BL) in the Tanana Valley is usually easterly or down the valley but is more complex in Fairbanks (Benson et al., 1983; Wendler and Nicpon, 1975). Wendler and Nicpon (1975) compared the low level inversions in Fairbanks with wind speeds and concluded that on average an inversion was present for wind speeds below 1.5ms^{-1} but for stronger wind speeds the inversion was broken up or disrupted. A northerly or northwesterly wind direction or calm is associated with the strongest inversions which is due to the gravity wind drainage from the surrounding hills under stable conditions.

Jayaweera et al. (1975) compared the sensible heat flux calculated from the wind and temperature profiles, S, with that estimated from the cooling of the atmosphere, K. Even though the values of S represent an upper limit for longer cooling periods they found that the value of K is higher than S. This was attributed to the drainage of cold air which contributes to about a third of the observed heat loss of the air layer above the valley. Also Benson et al. (1983) indicate that the winds can be variable in direction at different heights. These are cases in which the drainage winds generated on the surrounding hilltops may override lower, denser air layers. The winds above 400m approach the free air circulation above the hilltops.

The extreme low temperatures prevailing in the interior valleys of Alaska during winter are significantly modified by valley wind episodes which are driven primarily by synoptic scale surface pressure gradients along narrow valleys. Marvill and Jayaweera (1975) observed the warming of the valleys in the interior Alaska using the infrared

imagery of the NOAA-4 satellite, which provides an indicator of the radiative temperature of the emitting surface, and concluded that the valleys with winds are warmer than calm valleys. From hourly surface charts and twice daily satellite observations they found that the winds originate in the narrowest part of the river valley and spread along to the wide flats after they have developed substantially. The repeated initiation of the winds in these similar locations indicates the importance of the inter-play between the local topography and meteorology in the generation of valley winds. Thus when these winds are strong enough the surface temperature inversions that occur under clear sky conditions are broken, the warmer air aloft is brought to the surface by mixing, and the valley surface temperature rises nearly to that of the surrounding mountain top temperatures.

1.1.3 Urban heat island

The climate of cities is often quite different from that of the surrounding countryside due to a number of factors. First the energy consumption by factories, houses and automobiles generates waste heat, moisture, particles and gases that modify the climatic parameters in the city. Second the man made structures in the city have different reflectivities to sunlight and heat storage capacities than the surrounding landscape and forests (Benson et al., 1983). The Urban Heat Island is a term used to indicate the effect of a city on the temperature measured within the city. Its magnitude is measured by comparing the city temperatures with those of the surrounding countryside. Although Fairbanks is a comparatively small city, the per capita energy consumption is very high

because of the low temperatures, and the waste heat, moisture and pollutants are trapped by the low lying inversions and low wind speed (poor ventilation coefficient – product of BL height and wind speed inside the BL). Hence Fairbanks has a strong heat island effect in winters. According to estimates by Benson et al. (1983), using data from the Metropolitan Energy Use (from Landsberg, 1981), Fairbanks is the third highest per-capita consumer in the U.S, after Manhattan and Chicago. The winter heat island in Fairbanks frequently has a magnitude of 10°C, and magnitudes up to 14°C have been observed and their intensity correlated well with the intensity of the inversion in the lowest few tens of meters of the atmosphere (Bowling and Benson, 1978). In summer, energy consumption drops drastically because heating is no longer necessary and the lower inversions weaken or disappear. Hence the heat island effect also becomes weaker or disappears, except during nights when inversions are re-formed again.

1.1.4 Air pollution and ice fog

The meteorological conditions and the topography of Fairbanks, as described above, allow considerable pollutant buildup close to the ground in the city area. Carbon monoxide, oxides of nitrogen, lead, hydrocarbons and suspended particles are the principal pollutants of concern in Fairbanks and all exceed (by up to 1,500 %) the accepted standards for at least part of the year (Winchester et al., 1967; Gosink and Benson, 1982). The National Ambient Air Quality Standards (NAAQS) for carbon monoxide (CO) set by the U.S Environmental Protection Agency (EPA) are nine parts per million (ppm) for an eight hour average and 35 ppm for a one hour average.

According to the EPA report Fairbanks is the only serious CO nonattainment area with a population under 100,000 and little industry and that the CO limits were exceeded on more than 100 days per year in the 1970s. One of the reasons was the higher CO emissions of vehicles operating in cold temperatures. The annual 8-hour average was less than 3 ppm for the year 2006 due to the stringent emissions standards that have been followed through the years. Nevertheless, the previous scenarios illustrate the serious air pollution problems Fairbanks could face.

A considerable amount of water vapor is added directly to the air by the combustion of fuels for various purposes and indirectly from the cooling ponds of power generating plants. The saturation vapor pressure of air decreases rapidly with temperature and the excess water vapor freezes into very small droplets at temperatures below about -38°C forming ice fog. The particles in ice fog are almost spherical ice crystals. They are typically 5-20 μm in size and, as a result, can cause serious reductions in visibility (Benson et al., 1983). The ice fog is radiatively active in the thermal infrared and its absorption and re-radiating characteristics restrict the ground surface from acting as a radiating surface with respect to the atmosphere, and instead, the top of the fog layer becomes the principal radiator. Hence the inversion at the surface is lifted to the top of the fog layer and a neutrally buoyant boundary layer is formed close to the ground that allows free mixing of pollutants throughout the fog layer. Thus, pollutants such as carbon monoxide trapped at the surface diffuse throughout the fog layer but sulfur dioxide, emitted from tall smokestacks, is mixed down to the surface, increasing the concentrations near the ground (Holty, 1973).

The meteorological phenomenon and the air pollution problems described in the above sections are also applicable to many other high latitude urban communities. The effect of geographical and meteorological factors on transport and diffusion of air pollutants in these environments is of major concern.

1.2 SODAR and its applications

The SODAR (Sound Detection And Ranging) or acoustic sounder is a very useful instrument for studying the lower atmosphere because it can return valuable information on micro scale processes in the boundary layer. Sodars can be continuously and reliably used to measure the vertical profiles of wind speed and direction, vertical motions, turbulence and the thermal structure in the lower part of the troposphere. Briefly, the measurement of the above mentioned quantities is accomplished by emitting an acoustic pulse in the audio band and analyzing the backscattered echo. The time delay of the echo is used to measure the quantities as a function of height. McAllister (1969) first showed experimentally that acoustic echoes could be reliably obtained up to heights of several hundred meters.

The variations in the acoustic refractive index in the atmosphere, produced due to the fluctuations of temperature, vapor pressure and wind speed, are very large when compared to the variations produced in microwaves, which are used in radar. But the absorption of sound waves is typically several orders of magnitude higher than for microwaves. This limits the range of the Sodar typically to the lowest 1 to 2km of the atmosphere. The direct and strong interaction of sound waves with the microstructure of

the atmosphere, the low cost of antennas and the ease of installation are the factors that make the sodars useful instruments for studying the lower atmosphere. The theory and operating principles of the sodar will be described in chapter 2 of the thesis.

1.2.1 Acoustic sounder observations at Fairbanks in the past

The Geophysical Institute at the University of Alaska has operated an acoustic sounder before in cooperation with the National Oceanic and Atmospheric Administration (NOAA) wave propagation laboratory in Boulder, Colorado, during 1972 and 1973, the details and results of which are described in Holmgren et al. (1975). Some interesting observations from those studies are described below.

The Sodar was operated in the monostatic mode (see definition on page 11) with a repetition period of about 4 sec, corresponding to a tracking range of elevation of 600-700m, and a radiated acoustic power of 10 W. Facsimile plots are simultaneously generated giving a display of the height versus time variation of the backscattering intensity which is indicated by a grey scale. During strong inversions the acoustic records showed multi-layered structures, often with 10 to 20 separate quasi-horizontal backscattering bands from the surface up to about 450m, and often accompanied by waves of quite regular sinusoidal shape in phase throughout the sounding as well as others of more diffuse nature. The waves at higher elevations are broadened with streaks of echoes tilting to the left, generally associated with marked wind shears believed to be Kelvin-Helmholtz instability waves or breaking waves, which appear to induce marked wave trains decreasing in amplitude towards the surface. It is suggested that the strong

ground based inversions have a damping effect on the wave activity in the lower layers. The waves are often accompanied by transformation of the structure of inversion layer suggesting that the breaking waves induce effective mixing process.

The wind profiles taken alongside the sodar records, using balloon borne instruments, sometimes showed two or more low speed jets at different altitudes within the inversion layer flowing in almost opposite directions as well as a shearing layer near the top of the sounding. The backscatter bands were not consistently related to the regions of strong temperature gradients but on occasions correlated well with the wind shear layers and there was less backscatter from elevations corresponding to the maximum wind speed and calm regions between the jets. Thus during wave-breaking events the jets could be directly interpreted from the acoustic records.

The sodar used in the previous experiments conducted during 1972 and 1973 was a non-Doppler sodar. It only measures the intensity of backscatter which can be used to understand the turbulent structure in the atmosphere. However it is beneficial to have continuous vertical profiles of winds alongside the turbulence data. This can be accomplished by using a Doppler sodar which analyses the frequency content of the returned signal and thus provides the vertical profiles of wind speed and direction along with the turbulence data on a continuous basis. Based on this premise a commercially manufactured Doppler sodar was operated in Fairbanks, Alaska. The objective of this work is to explain the boundary layer phenomenon observed using the sodar during the winter under situations of strong temperature inversions.

Chapter 2 Theory and instrumentation

The Sodar used for this study is a REMTECH PA2 monostatic type Doppler Sodar, (PA meaning phased array), manufactured by REMTECH Inc. of France. The sodar basically consists of a single antenna, of the phased array type, and an electronic case. The antenna consists of an array of 196 elements or transducers mounted on four panels which are surrounded by sound absorbing cuffs to suppress side lobes and reduce unwanted background noise. The electronic case has a computer, transceiver and power amplifier.

In the monostatic mode of operation the transmitter and the receiver are collocated and hence the scattering angle is 180°. In our case the transmitter and receiver use the same antenna array. The sodar operates around a central frequency of 2250 Hz and an acoustic power of 10W. The typical range of the Sodar according to the manufacturer's specification is 1500m but this largely depends on the operating location and conditions. Parameters such as the averaging time, number of range gates, and the maximum range are operator selectable by simple key-in options on the computer. At the end of each averaging time, the sodar gives the vertical profiles of the temperature structure parameter C_T^2, horizontal wind speed in cm s^{-1}, horizontal wind direction in degrees, and the vertical wind speed in cm s^{-1}. At the end of each day the acquired data are automatically stored in the computer's hard disk in the form of text files. The following section provides a brief overview of how each of these quantities is measured by the sodar.

2.1 Estimation of C_T^2

When an acoustic pulse transmitted through the atmosphere interacts with an eddy its energy is scattered in all directions including back towards the sound source. The intensity or amplitude of the returned energy is proportional to the temperature structure parameter C_T^2 which is in turn related to the thermal structure and stability of the atmosphere. A more rigorous explanation of C_T^2 can be found on pages 13 and 14.

2.1.1 Scattering theory

The speed of sound in the atmosphere in relation to a fixed observer is a function of temperature, humidity, and wind speed. The fluctuation of these three quantities in the atmosphere results in the fluctuation of the refractive index of the atmosphere which in turn is associated with scattering of sound waves.

The changes in the refractive index may be expressed as fluctuations of wind and temperature, neglecting humidity fluctuations. Assuming a locally isotropic and homogeneous turbulence the theory of sound scattering, using the Born approximation, provides the following expression for acoustic differential scattering cross-section area per unit volume for unit solid angle (Batchelor, 1957; Tatarskii, 1971),

$$\sigma(\theta_s) = \frac{1}{8} k^4 \cos^2(\theta_s) \left[\frac{\phi_T(\chi)}{T_o^2} + \frac{\cos^2\left(\theta_s / 2\right) E(x)}{\pi c^2 \chi^2} \right], \qquad (2.1)$$

Where θ_s is the angle at the scattering volume from the transmitter beam axis to the receiver; k, the acoustic wave number; χ, the Bragg-scattering wave number equal to $2k\sin(\theta_s/2)$; T_o, the local temperature; c, the speed of sound; $\Phi_T(\chi)$, the isotropic three-dimensional spectral density of temperature; and $E(\chi)$, that of turbulent kinetic energy.

The first term in brackets in equation 2.1 represents the contribution to scattering due to temperature inhomogeneities and the second term represents the contributions from turbulent velocity fluctuations. As mentioned in the beginning of the chapter, for a monostatic sodar the scattering angle, θ_s, is 180°. Therefore the above equation reduces to

$$\sigma(\theta_s) = \frac{1}{8} k^4 \frac{\phi_T(\chi)}{T_o^2}. \tag{2.2}$$

That is, in monostatic mode the backscattering is due to random temperature fluctuations only.

According to Tatarskii (1971), the three-dimensional temperature spectrum can be expressed as

$$\phi_T(\chi) = 0.033\, C_T^2\, \chi^{-11/3} \tag{2.3}$$

Here C_T^2 is the temperature structure parameter given by

$$C_T^2 = D_T(r) r^{-2/3}, \tag{2.4}$$

where $D_T(r) = \left\langle [T(x+r) - T(x)]^2 \right\rangle$ is the temperature structure function in which the temperature is measured at points x and x+r and < > indicates an ensemble average.

Using the above expression for $\Phi_T(\chi)$, $\sigma(\theta_s)$ can be written as

$$\sigma(\theta_s) = \frac{0.033}{8} k^4 \frac{C_T^2}{T_o^2} \chi^{-11/3} \tag{2.5}$$

By substituting $\chi = 2k \sin(\theta_s)$ in Equation 2.5 we get

$$\sigma(\theta_s) \propto k^{1/3} \frac{C_T^2}{T_o^2} \tag{2.6}$$

2.1.2 Sodar equation

The sodar equation relating the radiated acoustic power P_e, to the received acoustic power, P_r, from height Z is given by (Little, 1969)

$$P_r = P_e A_e \frac{c\tau}{2} \frac{\sigma\alpha}{z^2}, \tag{2.7}$$

where A_e is the effective area of the receiving antenna; α the attenuation of the acoustic wave along the path; σ the cross-section of the scattering volume; τ the transmitted pulse width and c the speed of sound.

Therefore the received power depends on the scattering cross-section which in turn is a function of C_T^2. Thus the present sodar gives a unit-less value proportional to C_T^2 by calculating the ratio of received to transmitted power, taking into account the signal attenuation and the distance of propagation.

2.2 Wind speed and direction

In a Doppler sodar the measurement of the wind speed and direction is accomplished by analyzing the frequency content of the returned signal. The Doppler Effect, discovered by Christian Johann Doppler in 1842, is the change in frequency of a signal reaching a receiver when the receiver and the transmitting source are in motion relative to one another. The perceived frequency f' is related to the actual frequency f by

$$f' = f\left(\frac{v}{v \pm v_s}\right) \tag{2.8}$$

where v is the velocity of the wave in the medium and v_s is the velocity of the source.

In the case of the Doppler sodar, the source of the received signal is the scattering eddy moving along with the air and the change in the frequency produced by a scatterer is proportional to the rate of change of the distance between receiver and scatterer and the initial frequency. The received frequency will be greater than the transmitted frequency if the scatterer is moving toward the sodar antenna and is less when the scatterer is moving away from the antenna. Thus, for a known transmitted frequency, the received

backscattered wave frequency is measured and the motion of the scatterer relative to the transmitter receiver geometry can be calculated. For a monostatic sodar the Doppler shift corresponds to motions along the beam. Thus the determination of the three-dimensional wind vector requires multiple transmitter-receiver combinations, each sensing a different component of wind i.e. x, y and z.

The present sodar uses a phased-array antenna. This design enables the use of a single antenna for sequential monostatic soundings of the three-dimensional wind field. The system software controls the sequence and rate of operation of each beam. Electronic phase shifters apply a different phase shift to each antenna element to steer the beam. The shifted phase of each element causes the waves to interfere constructively, giving the maximum gain in the desired direction. Figure 2.1 is an illustration of the beam patterns showing the oblique and vertical beams used to sense the horizontal and vertical components of wind velocity. Up to nine beams can be achieved allowing cross checking among the wind components.

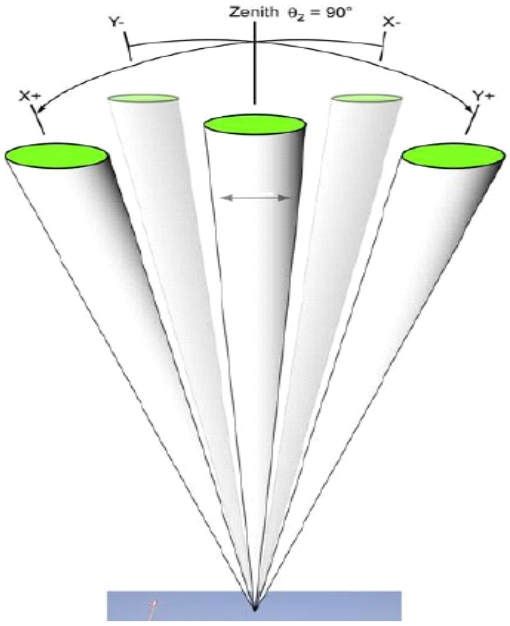

Figure 2.1 Vertical and oblique beams. Vertical and Oblique beams for measuring wind speed and direction. Four of the electronically steered beams are tilted from vertical and turned 90^{o} from each other to provide the horizontal component of wind velocity and one beam is pointed vertically and provides the vertical component of the wind. (Source: EPA QA Handbook of air pollution measurement systems Vol. 4: Meteorological Measurements, Version 1.0).

2.3 Sodar installation and data acquisition

The sodar was installed at the National Weather Service (NWS) site near the Fairbanks International Airport. Figure 2.2 shows the phased array antenna of the Remtech PA2 sodar at the site location. The system's hardware, consisting of a personal computer, a transceiver board and power amplifiers mounted in an electronics cabinet, are indoors in a temperature controlled environment.

Figure 2.2 Doppler sodar at the NWS site in Fairbanks. (Left) Doppler sodar antenna installed at the NWS site in Fairbanks. (Right) Closer look at the phased array antenna. It comprises of 196 transducers mounted on four panels and surrounded by sound absorbing cuffs to suppress side lobes and to reduce unwanted background noise. The three white heating cables seen on the right are passed along the base of the antenna elements to thaw the snow accumulated from precipitation. (Photos by the author).

Though the sodar was operated from the beginning of November 2005 to May 2006, useful data could only be obtained from the 8th of December 2005 due to a defective Data Acquisition (DAQ) card. Additionally, due to the extremely cold conditions and low turbulence in the lower atmosphere the data output, i.e. the measurements of the winds and C_T^2, were inconsistent with a lot of data missing at random intervals during the runtime. The beginning height of measurement was 50m and range bin increment of 15m to 50m and maximum recording height ranging from 1000m to 1500m were used as the input settings for the sodar during the period of operation. The sodar was operated with

different averaging times ranging from 5 to 30 minutes with longer averaging times used during cold conditions and when the sodar was giving missing data.

After every averaging interval the computer displays the processed data in a tabular form. This processed data is obtained automatically by applying Fast Fourier Transforms (FFT) to the received signal. No access to the raw data was provided by the manufacturer. The system software provides a signature to the transmitted pulse by emitting 9 frequencies serially, which causes the sodar to make a singing noise while in operation. The coded pulse is easier to detect from noise and fixed echoes upon reception. At the end of each day, at 12:00 AM, all the processed data is automatically stored in the form of text files in the computer's hard disk. These text files were frequently transferred to a USB memory stick and backed up to be used for plotting and data analysis. No additional data processing was performed.

2.4 Sodar dataset and additional sources of data

The sodar data obtained between December 2005 and April 2006 was used for the analysis in this work. Height versus time plots of the horizontal wind speed and direction, vertical wind speed and C_T^2 were generated from the text files using Interactive Data Language (IDL). Figure 2.3 shows the time versus height plot of the unit-less value of C_T^2 measured by the sodar on 9 December 2005 from 00:00 to 12:00 Alaska Standard Time (AKST = GMT - 9 hours). The wind speeds and direction were similarly plotted. The higher values of C_T^2 between the altitudes of 100m to 200m corresponds to a strong inversion layer extending from the surface to 250m AGL with a temperature difference of

11°C as seen in the temperature profile shown on the right. The temperature profile is plotted from the high resolution radiosonde data. The white vertical line on the sodar profile indicates the radiosonde launching instant. An averaging time of 15 minutes was used on this day for the sodar recordings. The resolution in profiles plotted from the averaged data differs from those plotted with non-averaged data.

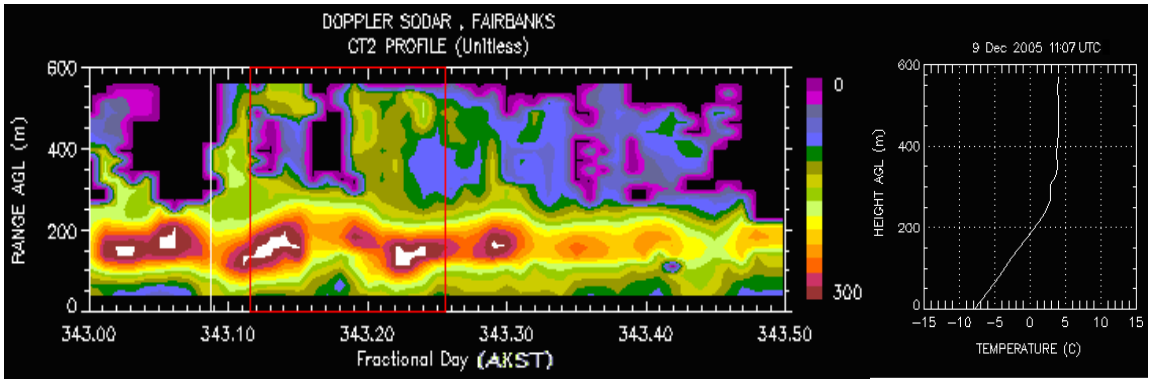

Figure 2.3 Example of C_T^2 profile from sodar. (Left) Time vs. height plot of C_T^2 obtained from the sodar on 9 December 2005 from 00:00 to 12:00 AKST. The abscissa shows the fractional Julian day and the ordinate shows the height in m AGL. The magnitude of C_T^2 is indicated on a color scale ranging from 0 to 300. The white vertical line in the profile shows the radiosonde launching instant and the black region within the box represents the altitudes for which no values could be obtained by the sodar while it was operating. (Right) Temperature profile from the high-resolution radiosonde data taken at 02:07 AKST the same day. The abscissa shows the temperature and the ordinate shows the height AGL.

Figure 2.4 shows the non-averaged profile of the backscatter intensity recorded on 26 February 1973 between 02:48 and 06:08 local time using a non-Doppler sodar operated in the mono-static mode in Fairbanks. The time duration of the profile shown in Figure 2.4 is indicated by the red box on the profile shown in Figure 2.3. This allows a

comparison between the resolution provided by the non-averaged and averaged sodar profiles.

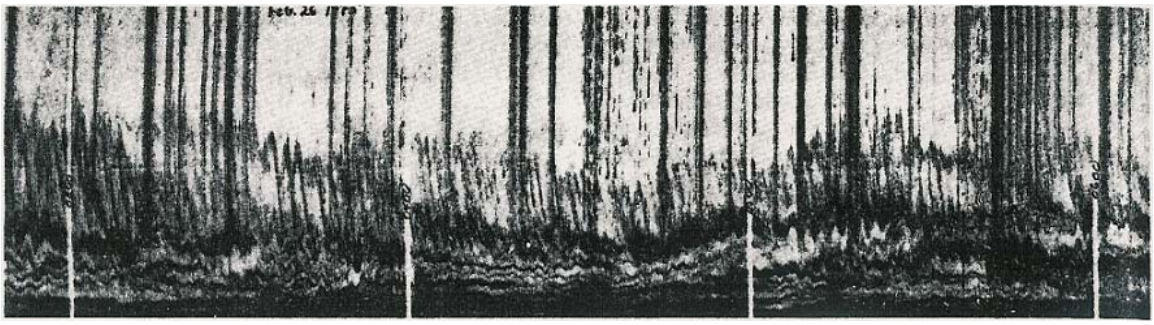

Figure 2.4 Facsimile plot of acoustic sounding in Fairbanks in past. Facsimile record of the backscatter intensity recorded on 26 February 1973 between 02:48 and 06:08 local time using a non-Doppler sodar operated in the mono-static mode in Fairbanks. The intensity of backscatter is indicated on a grey scale. The distance from the bottom to the top of the record corresponds to about 650m. The quasi-horizontal bands are the backscattering echoes. The vertical lines are due to traffic noise. (Source: Holmgren et al., 1975)

In order to substantiate the sodar data for further analysis, surface pressure plots and cloud cover observations were obtained from the Local Climatological Data set of NWS station operated by the National Oceanic and Atmospheric Administration (NOAA). Twice daily radiosonde data with a 6-s resolution for Fairbanks station was obtained from the National Climatic Data Center (NCDC) for high resolution vertical profiles of temperature, winds and humidity. The dataset undergoes the standard quality control (QC) process at UCAR with no additional QC performed at NCDC. The received data is processed by NCDC and converted to the final ASCII archive files by using the software

provided by University Corporation for Atmospheric Research (UCAR)/ Joint Office of Science Support (JOSS). No additional processing of data was done.

The NWS station at Fairbanks is at an elevation of 135m above Mean Sea Level (MSL). Fig. 2.5 shows the profile of the temperature versus height Above Ground Level (AGL) plotted from the radiosonde data obtained at 00 UTC on December 15th 2005. A temperature inversion can be observed starting from the surface to a height just under 100m over which a near isothermal layer extends to a height of 900m. Above this there is an elevated layer of inversion extending to approximately 1200m. Though the inversion layers can be detected by visual inspection of the temperature profile plots, using an algorithm to detect the inversion layers is more beneficial since the other quantities corresponding to the layers of inversion can be obtained simultaneously and because it offers a consistent interpretation of the plot.

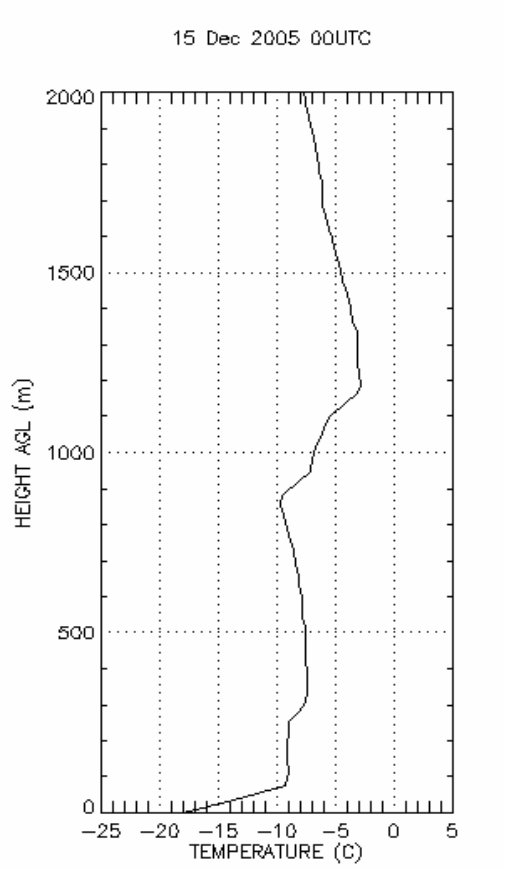

Figure 2.5 Temperature profile from the high resolution radiosonde data. The abscissa shows the temperature in °C and the ordinate shows the height in m AGL. A surface based inversion extends up to 70m AGL above which two layers of elevated inversion are present extending approximately from 260m to 310m AGL and 880m to 1190m AGL.

2.5 Algorithm to detect strong layers of temperature inversion

The high resolution radiosonde data received from the NCDC is in ASCII format with twice daily sounding data for the entire month stored in a single file. These files were broken down into individual files for each sounding and stored in NetCDF format. An algorithm was developed to detect strong layers of inversion by scanning the temperature profiles from the sounding. The stepwise process in the algorithm is as follows

1. Read the NetCDF file for a particular sounding and store the temperature, dew point temperature, Relative humidity, wind speeds and direction for the corresponding altitudes in the sounding in a tabular form.
2. Beginning from the surface the temperature profile is scanned upwards looking for an increase in temperature with altitude at a rate $\geq$ 1°C/100m. The first point encountered meeting this condition is stored in an array 'inv_B' representing the base of the inversion layer.
3. Following the array point recognized in step 2 the temperature profile is now scanned upwards looking for a point where the temperature increase with altitude decreases to less than 1°C/100m and this point is stored in an array 'inv_T' representing the top of the inversion. Repeat step 2 starting from the array point recognized in step 3.
4. Steps 2 and 3 are repeated until the end of file is encountered thus resulting in two arrays 'inv_B' and 'inv_T' containing the base and top of however many inversion layers may be present.
5. If the separation between two consecutive layers of inversion is less than 100m then the negative lapse rate layer between them is ignored and is considered to be within a deeper inversion layer. The two inversion layers are merged together into a layer whose base is taken as the base of the first layer and the top being the top of the higher inversion layer. Thus two new arrays are created.
6. From the arrays created from step 5 only the layers with a temperature difference greater than 2°C are retained, thus filtering the arrays to isolate the strongest inversions.

In the above steps the application of the constraint '1°C/100m' for detecting the layers of inversion and eliminating inversion layers with a temperature difference less than 2 °C was done in order to eliminate the detection of the near isothermal layers that may be present and to detect only strong inversion layers. The values of the above mentioned constraints were chosen through trial and error method by visually inspecting the resulting plots from the algorithm for the cases where the algorithm failed to give the desired results. Figure 2.6a shows the temperature profile from Figure 2.5 with four inversion layers detected after step 4 of the algorithm. The stars on the profile represent the base of the inversion layers and the diamonds represent the top of the inversion layers. The final inversion layers detected after steps 5 and 6 are shown in Figure 2.6b. The inversion layer extending from about 250m to 300m shown in Figure 2.6a was eliminated since it is less than 2 °C. The two layers of inversion on the top of Figure 2.6a were merged into a single layer as the separation between them is less than 100m. The algorithm also gives the altitudes and the corresponding temperatures of the final inversion layers in a tabular form as shown in Figure 2.6c. The first layer extends from the surface to 74m AGL and the elevated layer extends from 881m to 1187m AGL. The corresponding temperature differences across the first and the second inversion layers are 8.7 °C and 6.7 °C respectively.

The algorithm can be run in a batch fashion for multiple soundings with the output plots and tables for each sounding in the batch stored as separate files.

(a) **(b)**

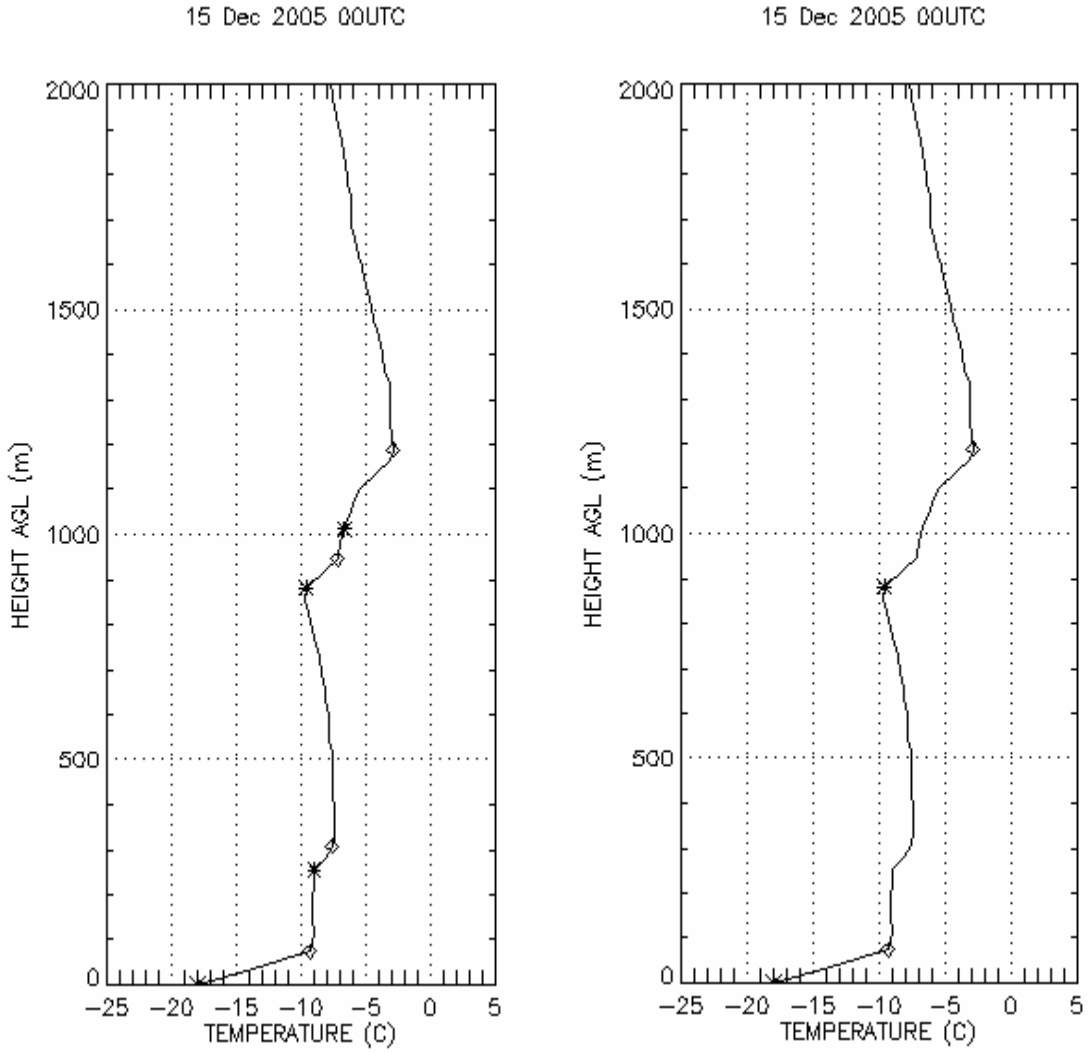

(c)

Sounding Date_Time:	20051215_00	
Height of the Inversion Base:	0.000000	881.000
Height of the Inversion Top:	74.0000	1187.00
Temperature at the Inversion Base:	-18.0000	-9.60000
Temperature at the Inversion Top:	-9.30000	-2.90000

Figure 2.6 Inversion layers detected by the algorithm. (a) Temperature profile showing the four inversion layers initially detected by the algorithm. The * represents the base and the ◊ represents the top of the of the inversion layers (b) Final two inversion layers selected by algorithm (c) Altitude and temperature data for the two inversion layers shown in Fig. 2.6b.

Chapter 3 Results and discussion

The results from the inversion detection algorithm can be used to describe the variation in the surface temperatures and the characteristics of the temperature inversions for the periods overlapping the sodar data set.

3.1 Results from the inversion detection algorithm

The algorithm was applied to the radiosonde data from December 2005 to April 2006, over the period the sodar was operated. This time period is sufficient to provide an overview of the variation of the inversion characteristics from the coldest months in winter to late spring when there is more available sunlight and the diurnal variation is more pronounced. Out of the several layers of inversions that may be detected in a sounding, starting from the ground, only the lowest layer within 1500m AGL was used in this analysis. Figure 3.1 shows the surface temperatures obtained from the twice daily radiosonde launches. The coldest temperatures can be seen more frequently in the months of December and January. The variances in the plot are closer as we move towards March indicating the increasing diurnal variation in temperatures due to the increasing hours of daylight.

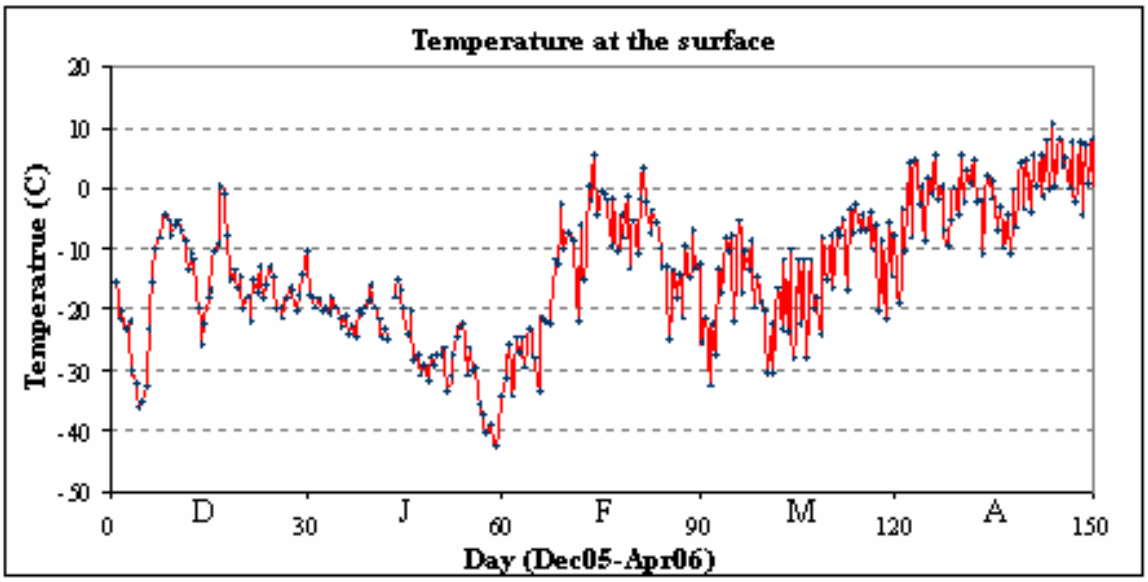

Figure 3.1 Surface temperatures from radiosonde observations. Surface temperature obtained from the twice daily radiosonde data for Fairbanks from December 2005 to April 2006. The ordinate shows the month and day while the abscissa shows the temperature in °C.

Figure 3.2 shows the base of the inversion layers, their extent and the temperature difference across the layers. Also, for each plot lines of best fit, generated using a fourth order polynomial, and their equations are shown. The inversions are stronger, deeper and more frequent during the winter time and are mostly surface based. As we proceed towards warmer months, both the strength and extent of inversions decrease with elevated layers being more common.

Figures 3.2 (b) and (c) show that even during the winter months in some cases the inversion layers on a few soundings are much smaller and weaker than the ones often observed in winter. This is because the algorithm neglects the near isothermal layers, in which the temperature increase with height is less than 1°C/100m that may be present

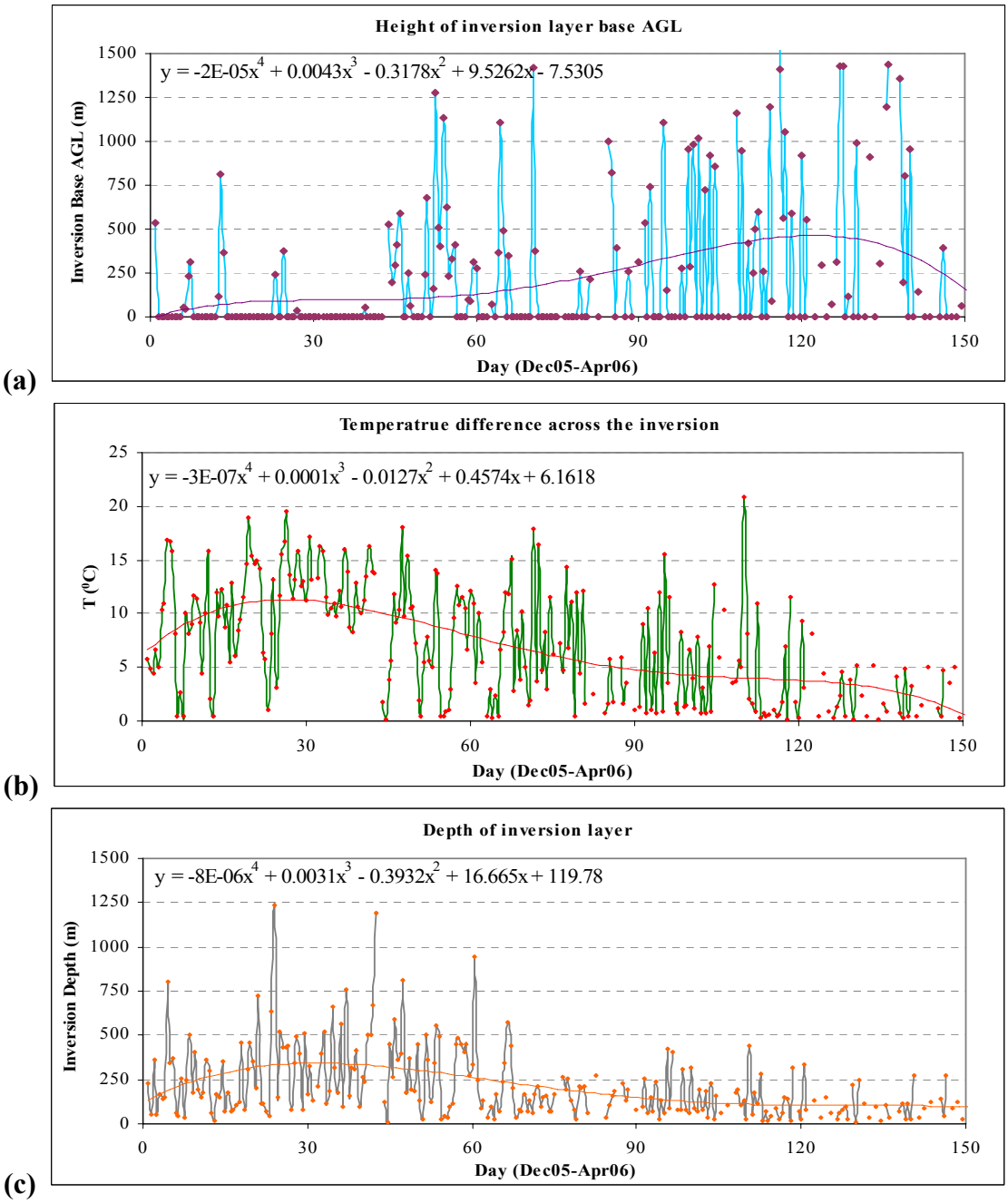

Figure 3.2 Characteristics of the inversion layer. Characteristics of the lowest inversion layer obtained by the inversion detection algorithm using the twice daily radiosonde data from December 2005 to April 2006. (a) Height of the inversion layer base AGL, (b) temperature difference across the inversion layer and (c) depth of the inversion layer. Also for each plot lines of best fit, generated using a fourth order polynomial, and their equations are shown.

above or below the detected inversion layer. Thus the algorithm shows only the strong sections of a long inversion layer that may be near isothermal throughout with a few strong layers embedded in them. This can be said to be a draw back of the algorithm arising in cases as described above, but as shown in the following sections the algorithm successfully captures the variations in the inversion characteristics with variations in other parameters.

3.1.1 Diurnal variations in inversion characteristics

The results from the algorithm that are shown in Figures 3.1 and 3.2 were plotted separately for soundings taken during day and night to analyze the diurnal variation in the characteristics of the inversion layers. The 00 UTC sounding is taken as day time sounding when it is 3:00 PM AKST and the 12 UTC sounding is taken as the nighttime sounding when it is 3:00 AM AKST.

Figure 3.3 shows the surface temperature plotted separately for day and night. The contrast between day and night temperatures is negligible during the winter months due to the few hours of available sunlight during the day combined with the low solar elevation angles. The contrast increases from late winter to late spring due to the increasing hours of available daylight. Similar patterns could be observed in the inversion characteristics as shown in Figure 3.4. The strength and depth of the inversions are similar both for day and night during the winter months. Starting from early February the inversions during the nights are much stronger and deeper than the ones during the day time.

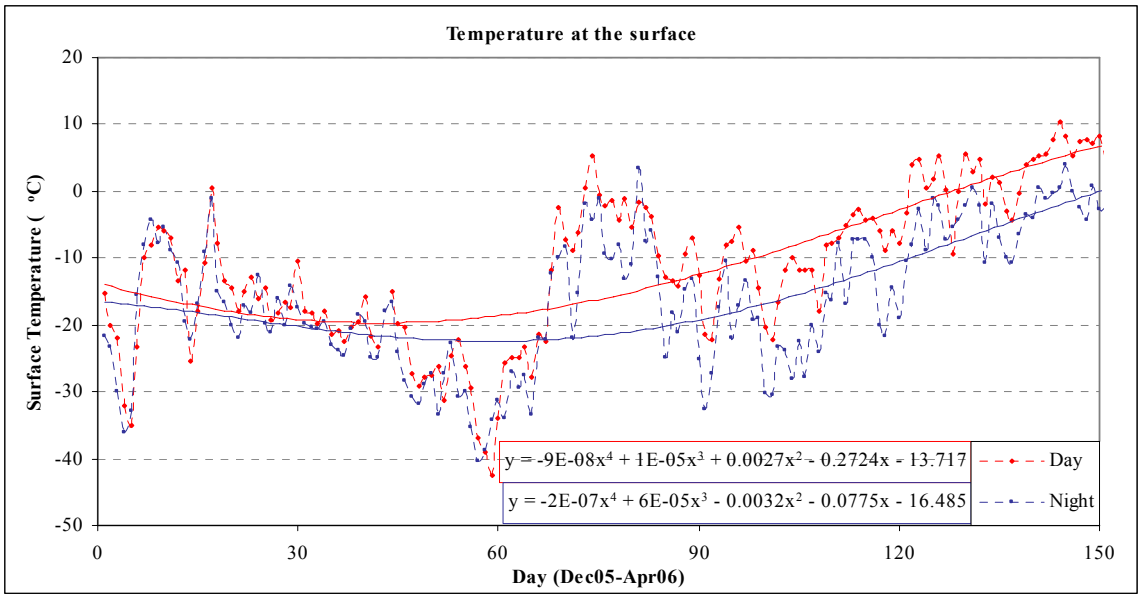

Figure 3.3 Surface temperatures for day and night. Surface temperatures obtained from the radiosonde data from December 2005 to April 2006 plotted separately for day and night. Temperatures during the night are shown in blue and the ones during the day are shown in red.

The increased available sunlight during the day heats up the ground which in turn heats the air above it thus weakening the inversion and sometimes destroying the inversion layer near the ground resulting in an elevated layer of inversion above the ground. This can be observed in Figure 3.5 which shows the height of the inversion base for both day and night. During the winter months most of the inversions are surface based and occurrences of elevated inversions are rather uncommon with their frequencies being similar during day and night. Starting from February most of the inversion layers are still surface based during the night but are elevated during the daytime.

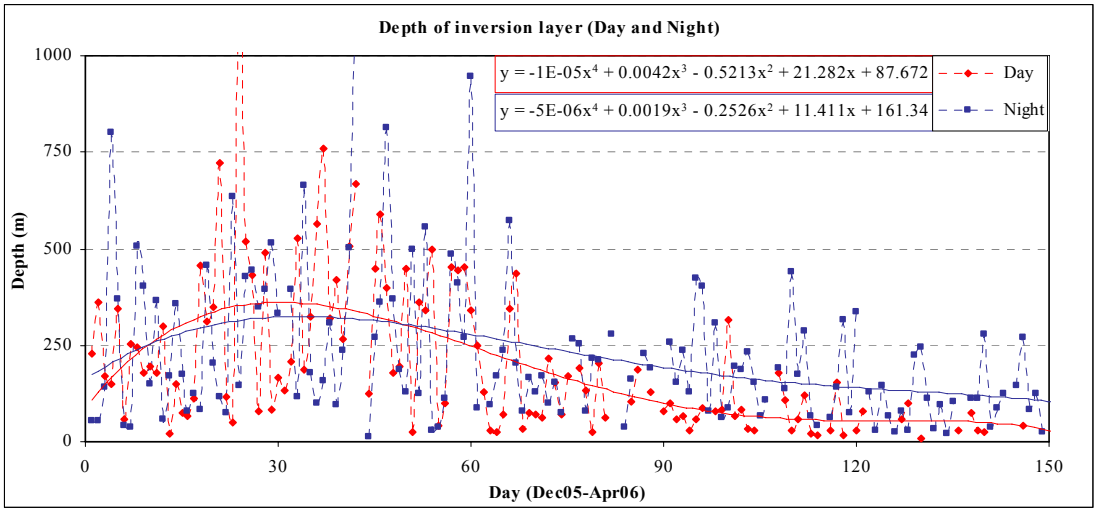

(a)

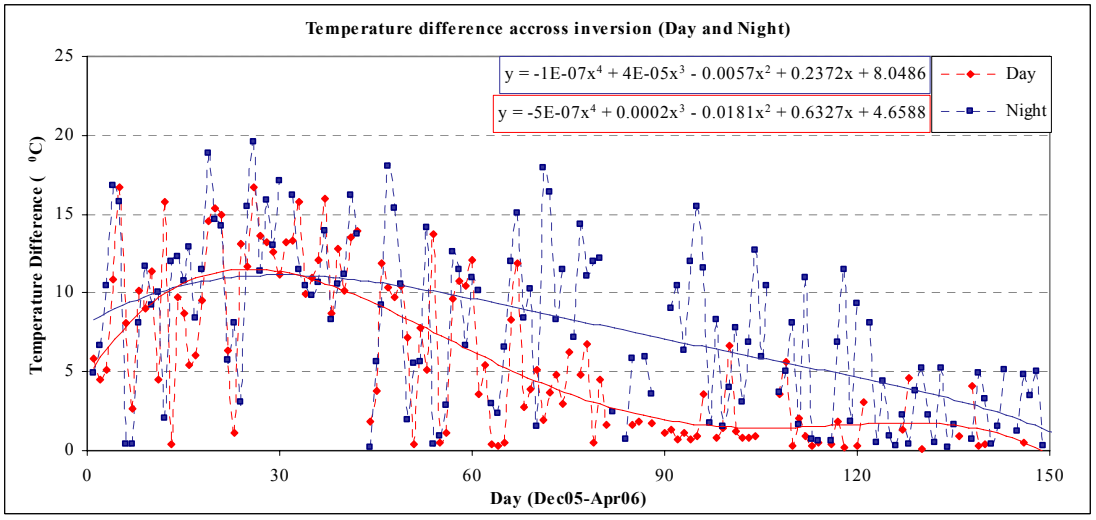

(b)

Figure 3.4 Characteristics of the inversion layer for day and night. Characteristics of the lowest inversion layer shown in Figure 3.2 plotted separately for day and night. (a) Depth of the inversion layer and (b) temperature difference across the inversion layer.

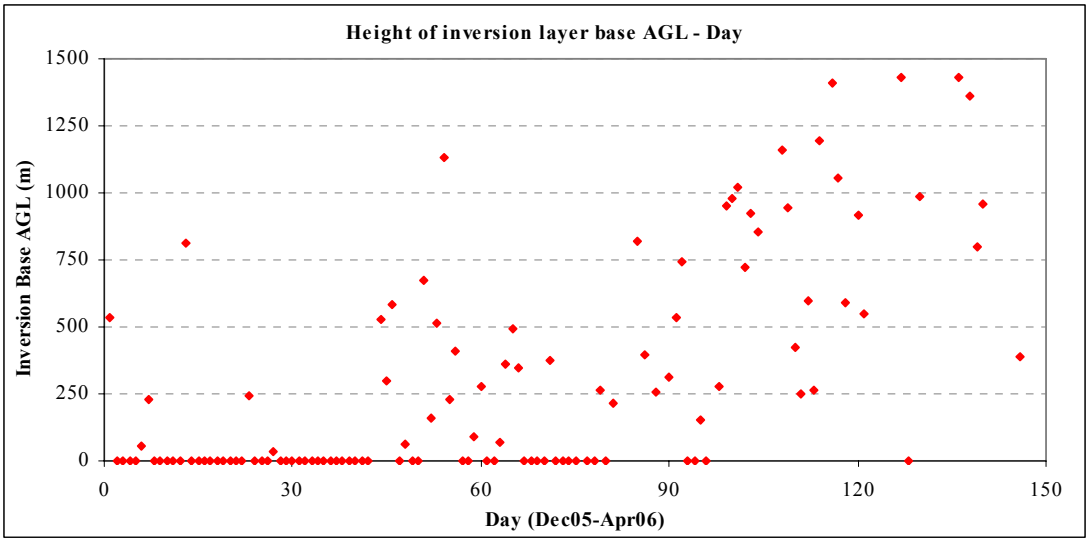

(a)

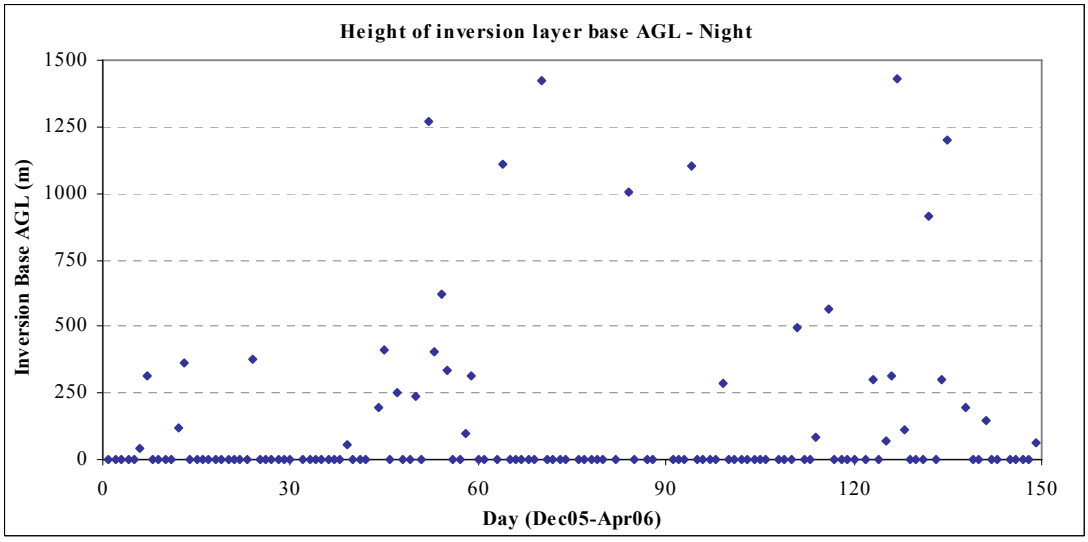

(b)

Figure 3.5 Height of the inversion layer base AGL - day and night. Height of the inversion layer base AGL shown in Figure 3.2 plotted here separately for (a) day - shown in red and (b) night - shown in blue.

3.1.2 Effect of cloud cover on inversion characteristics

The incoming solar energy absorbed by the earth-atmosphere system is re-emitted to space. Just as the sun emits electromagnetic radiation covering all frequencies, so do the earth and the atmosphere but the intensity peak of this radiation field is in the longer wavelengths, i.e. in the thermal infrared region.

The presence of clouds affects the radiation budget of the earth-atmosphere system and hence the surface temperatures. On the one hand, they reflect a significant portion of the incoming solar flux, and on the other, they trap the outgoing thermal Infra Red (IR) fluxes emitted from the atmosphere below the clouds and from the surface. The competition between these two effects determines whether the surface will undergo cooling or warming (Liou, 2002). In the absence of sunlight only the latter effect of clouds comes into play thus causing a decrease in the net outgoing radiation and an increase in surface temperatures. Thus, during nights and polar winters, when solar radiation is absent, variations in cloud cover have marked effect on the inversion layer.

The characteristics of the inversion layers obtained from the algorithm were analyzed separately for clear and cloudy conditions in order to examine the cloud effects. The cloud cover data set contained cloud observations at 3-hour intervals for the period of December 05 to April 06. Sky cover values (amount of sky obscured) of $\leq 2/8$ are treated as clear and $\geq 5/8$ are treated as cloudy. In choosing the clear and cloudy cases the cloud conditions during the nighttime sounding were used when there is no solar radiation and the cloud effects on the inversions are more apparent. The corresponding daytime

soundings for the chosen nighttime soundings were compared together for changes in the inversion characteristics.

Out of the 151 days from the beginning of December 05 to the end of April 06, 67 cloudy nights and 60 clear nights were chosen for analysis. Figures 3.6 (a) and (b) show the surface temperatures plotted for day and night, obtained from the radiosonde soundings, for the chosen clear and cloudy nights respectively. Comparing the temperatures for clear and cloudy cases, it can be seen that from early spring the nighttime temperatures are much colder than the daytime temperatures during clear conditions than the cloudy conditions. During the nights, in the absence of incoming solar radiation there is a net loss of heat from the ground because the Earth still emits heat in the form of IR radiation. Hence the nights are usually colder than the days. With the presence of clouds some of the outgoing IR radiation is reflected back to the ground thus decreasing the net heat loss from ground. Hence the diurnal variation in surface temperatures is much smaller during cloudy conditions than clear conditions. Using the results from the algorithm it is calculated that the average temperature difference between day and night, from mid February to end of April, is 9.7 °C for clear conditions and 5.3 °C for cloudy conditions.

Similar cloud effects can be seen on the inversion characteristics. Figure 3.7 shows the temperature difference across the inversion plotted for clear and cloudy conditions. Beginning from early spring the inversions during the nights are found to be much stronger than the daytime inversions during clear conditions. These diurnal changes in temperature and inversion characteristics are not so apparent in the winter months due to

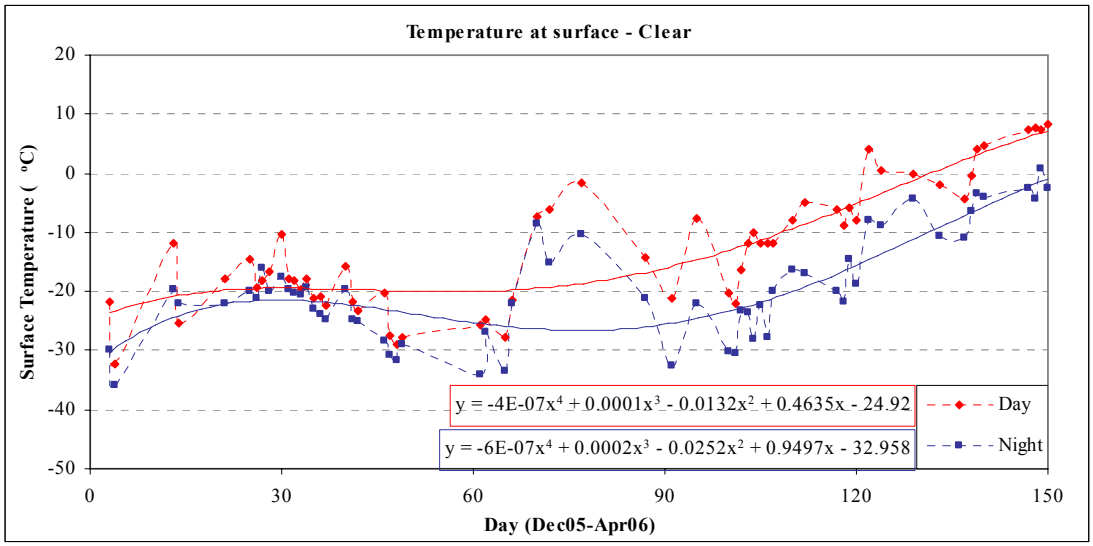

(a)

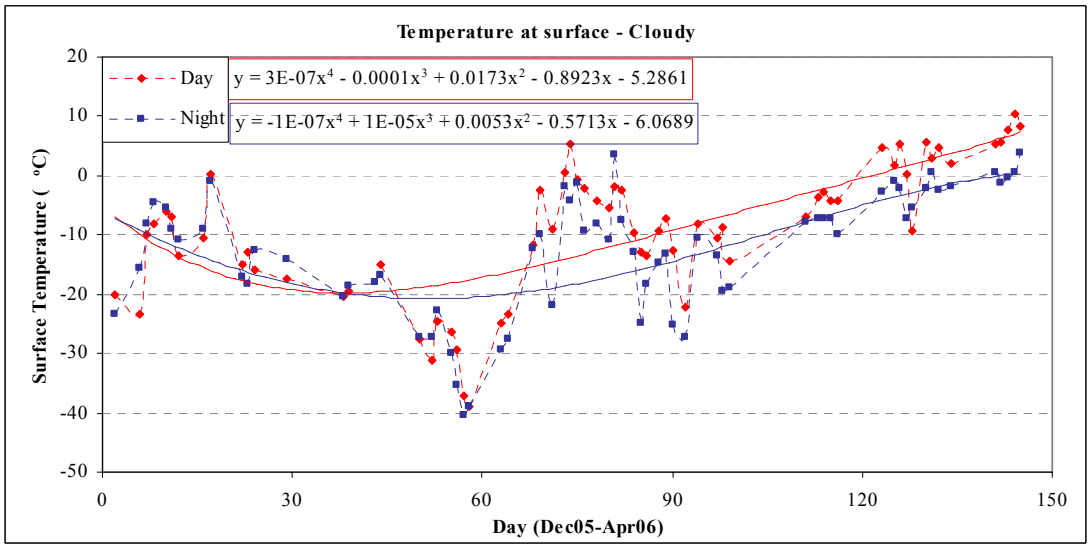

(b)

Figure 3.6 Surface temperatures for clear and cloudy conditions. (a) The surface temperatures for the chosen clear nights are shown in blue and the corresponding daytime temperatures for those clear nights are shown in red. (b) Surface temperatures for the chosen cloudy nights are shown in blue and the corresponding daytime temperature for those cloudy nights are shown in red.

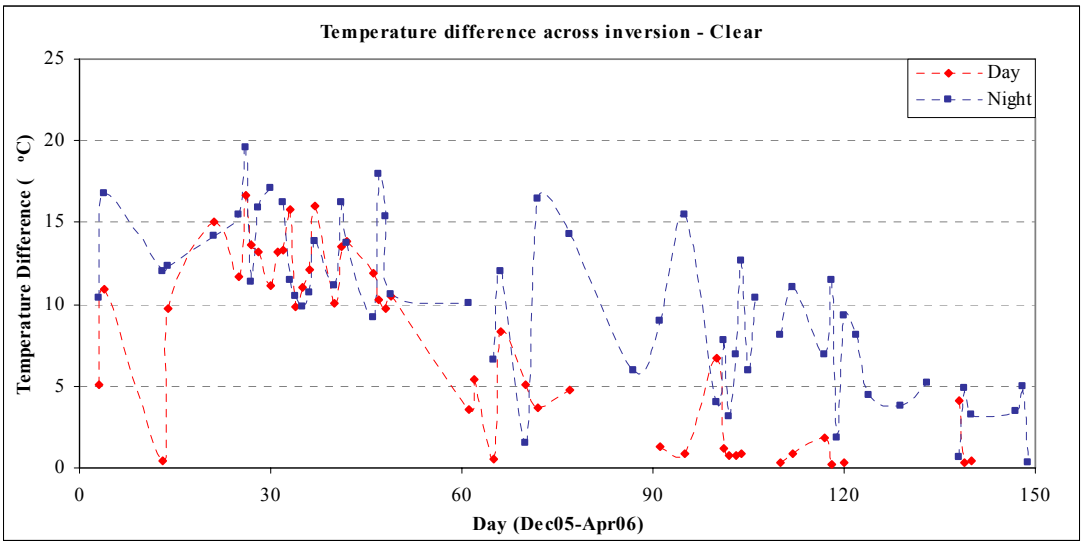

(a)

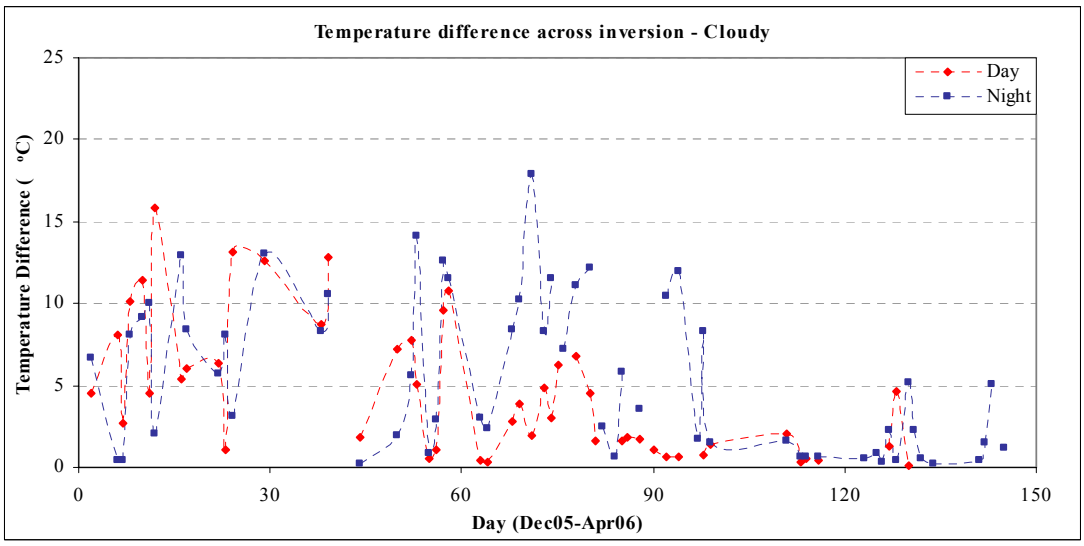

(b)

Figure 3.7 ΔT Inversion for clear and cloudy conditions. (a) Temperature difference across the inversion during clear nights is shown in blue and the corresponding daytime values are shown in red. (b) Temperature difference across the inversion during cloudy nights is shown in blue and the corresponding daytime values are shown in red.

the little amount of sunlight available during the day to heat the ground causing a rise in the surface temperatures.

The surface heating produced by the clouds can cause a surface based inversion to be destroyed resulting in an elevated inversion layer. This can be seen in Figure 3.8 which shows the base of inversion layer for cloudy and clear nights. On clear nights most of the inversions are still surface based even in the relatively warmer months of March and April unlike cloudy nights in which a majority of inversion layers are elevated in the warmer months with some elevated layers found even during the colder winter months.

3.2 Wind observations from sodar data

The wind observations recorded by the sodar between December 05 and April 06 are presented in this section. Although the sodar records the data at different altitudes of fixed increments, in order to present the statistics of the winds near the surface over this time period and to compare their seasonal variation, the lowest data point was retained for analysis. The minimum starting altitude of the sodar is 50m making it the data point closest to the ground. However, the data from the first point are sometimes unreliable and hence the data immediately above the 50m level was retained instead. Range bin sizes of 20 and 25m were used during the recording period and hence the data presented in this section is from either 70m or 75m AGL.

Figure 3.9(a) shows the sodar observations of wind speed and direction, at the end of the averaging periods coinciding with the twice daily radiosonde launch times, between December 05 and April 06 plotted in the form of wind roses. The recordings are from an

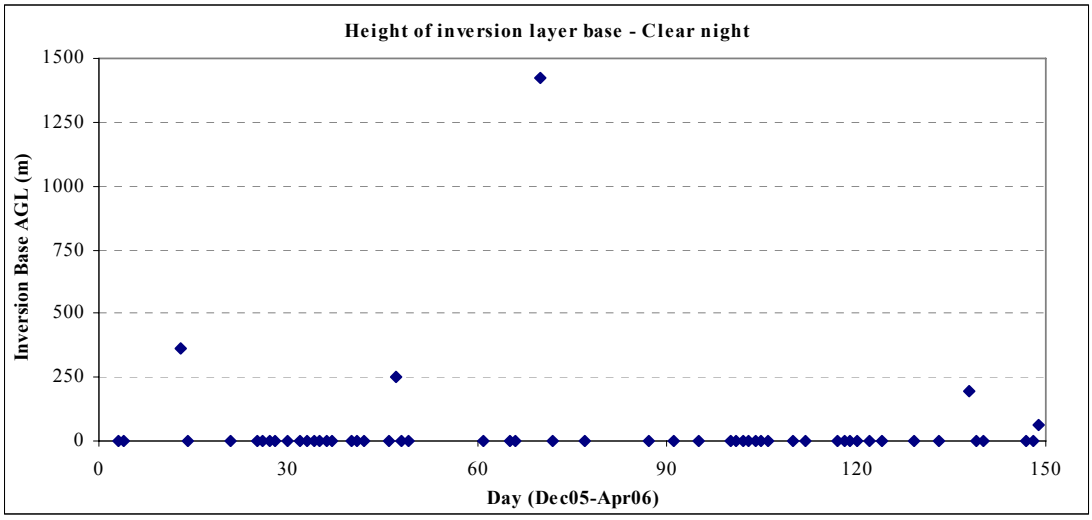

(a)

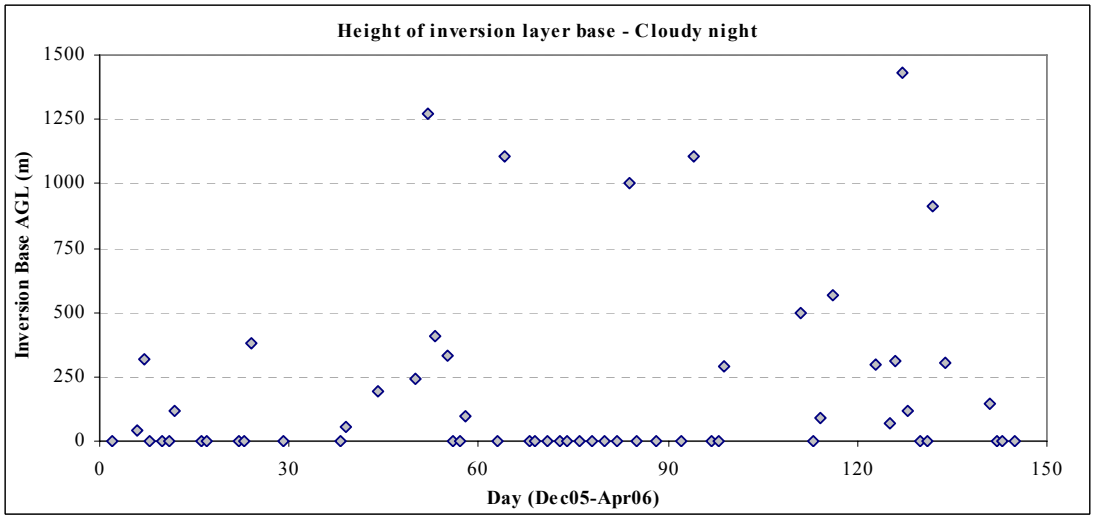

(b)

Figure 3.8 Height of the inversion layer base AGL based on cloud conditions. Height of the inversion layer base above ground plotted separately for (a) clear nights and (b) cloudy nights.

average altitude of 70m AGL. A total of eight petals are used with each indicating a particular direction such as North (N), North-East (NE), East (E) and so on depending upon their position. The wind rose shown in Figure 3.9 (b) was generated, using the same parameters as the sodar wind rose, from the twice daily radiosonde observations over the same time period to compare with the sodar observations. The altitudes of radiosonde observations do not coincide exactly with that of the sodar and hence the radiosonde winds from an altitude closest to the sodar recording altitude were used.

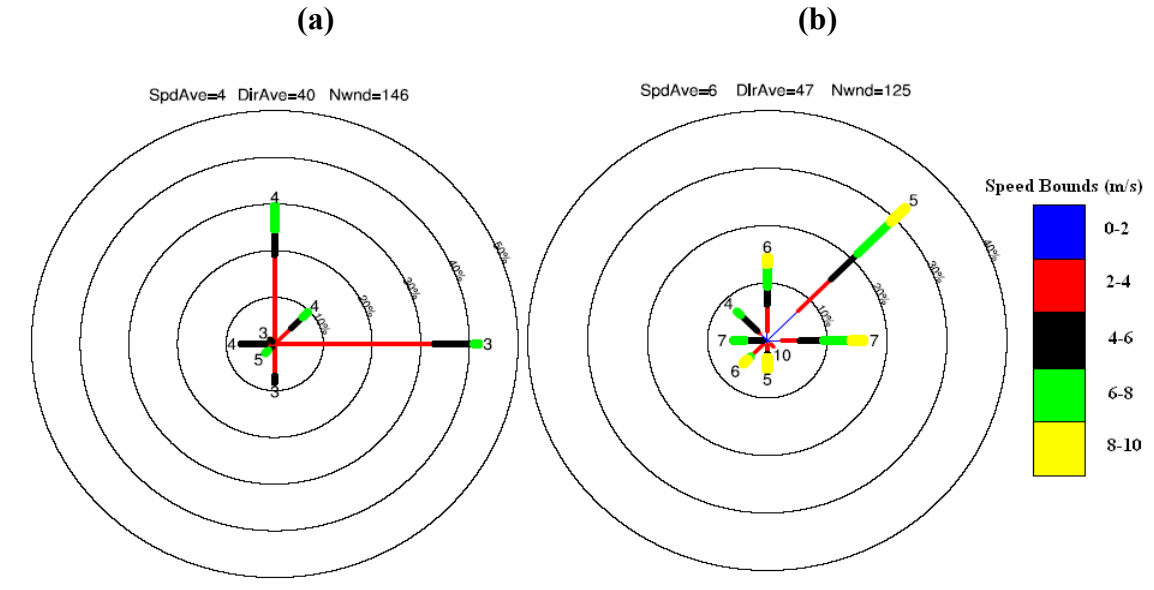

Figure 3.9 Wind roses from sodar and radiosonde data. Wind roses plotted using twice daily observations at an average altitude of 70m AGL from (a) sodar and (b) radiosonde between December 05 and April 06. The circles indicate the frequency percentage of the winds and the length of each petal is representative of the frequency percentage of winds from a particular direction. Each color on the petal represents a particular speed bound as shown on the right of the figure and the length of each colored line on the petal gives the fraction of total frequency of winds flowing from that direction falling into a particular speed bound. The average speed of the winds flowing from a particular direction is given at the end of the petal.

It can be seen from Figure 3.9 (a) that the majority of the winds are from the N, NE or E which is in good agreement with the radiosonde data. The easterly flow is a part of the large scale air drainage down the Tanana Valley under strong inversion conditions which can be modified by the semicircle of hills that surround Fairbanks as suggested by Benson and Weller (1969). Also the greater frequency of the northerly flow is due to the gravity wind drainage that occurs from the surrounding hills under stable conditions. The comparison of the wind roses from the sodar and the radiosonde data suggests that there is a good agreement in the wind directions but the sodar underestimates the wind speed by about 2 ms^{-1}. This might be due to the averaging of data involved in the sodar measurements.

Figure 3.10 (a) and (b) show the wind roses plotted separately for each month using the same data as in Figure 3.9. Though the majority of the winds are still from the N, NE or E it can be noticed that the frequency of winds from other directions increases in the warmer months. A possible explanation is that as the inversions become weaker and less frequent the drainage winds down the Tanana Valley also become weaker and less frequent. The sodar operates on a continuous basis and hence is able to provide data at more frequent intervals. The wind roses from the sodar observations at one hour intervals are shown in Figure 3.11. The wind data at more frequent intervals compares well with that shown in Figures 3.9 and 3.10 validating that the sodar can be used as a reliable source of frequent wind observations.

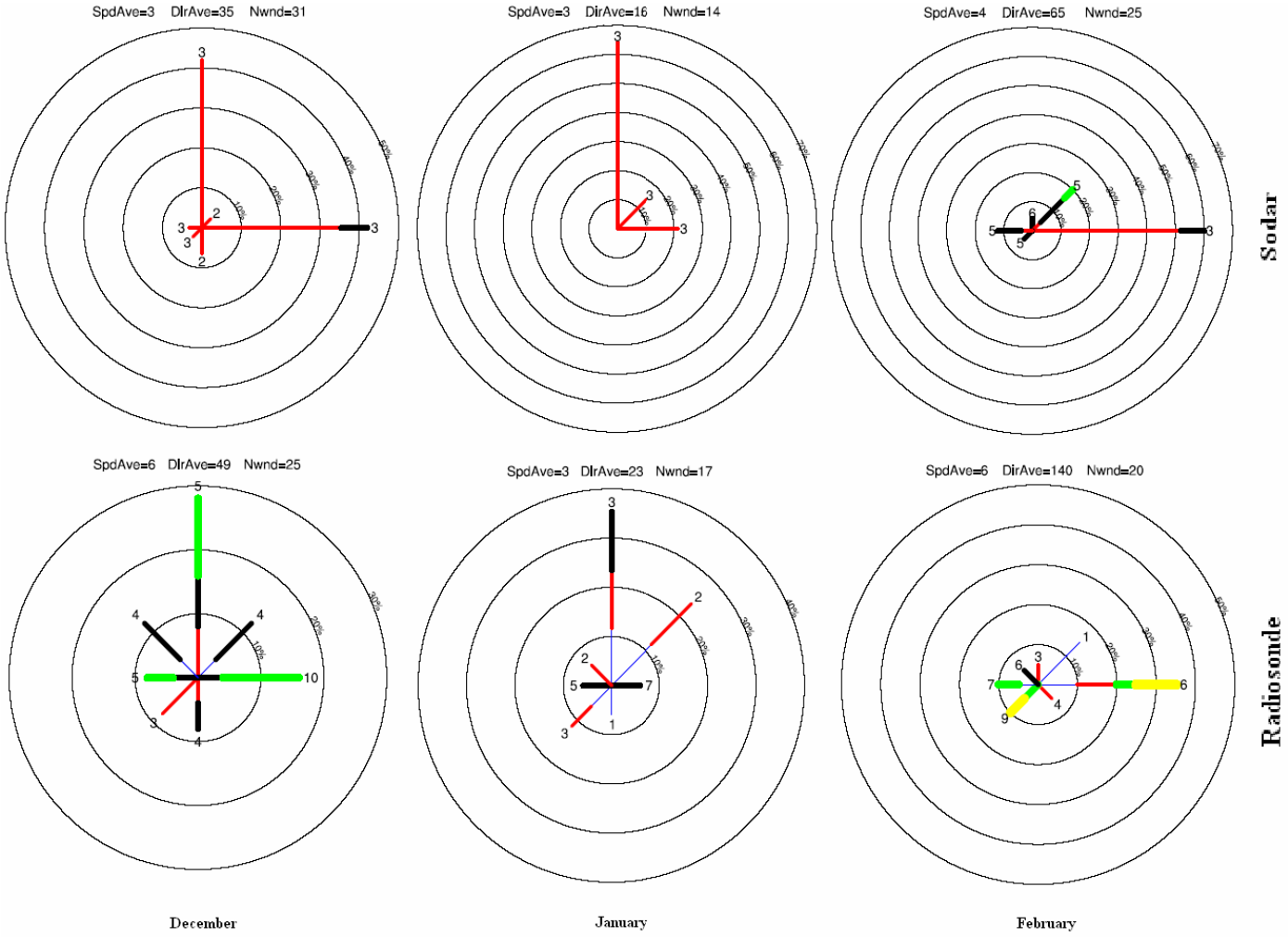

Figure 3.10a Wind roses - month wise. (a) Wind roses plotted separately for the months of December, January and February using the same data as in Fig. 3.9.

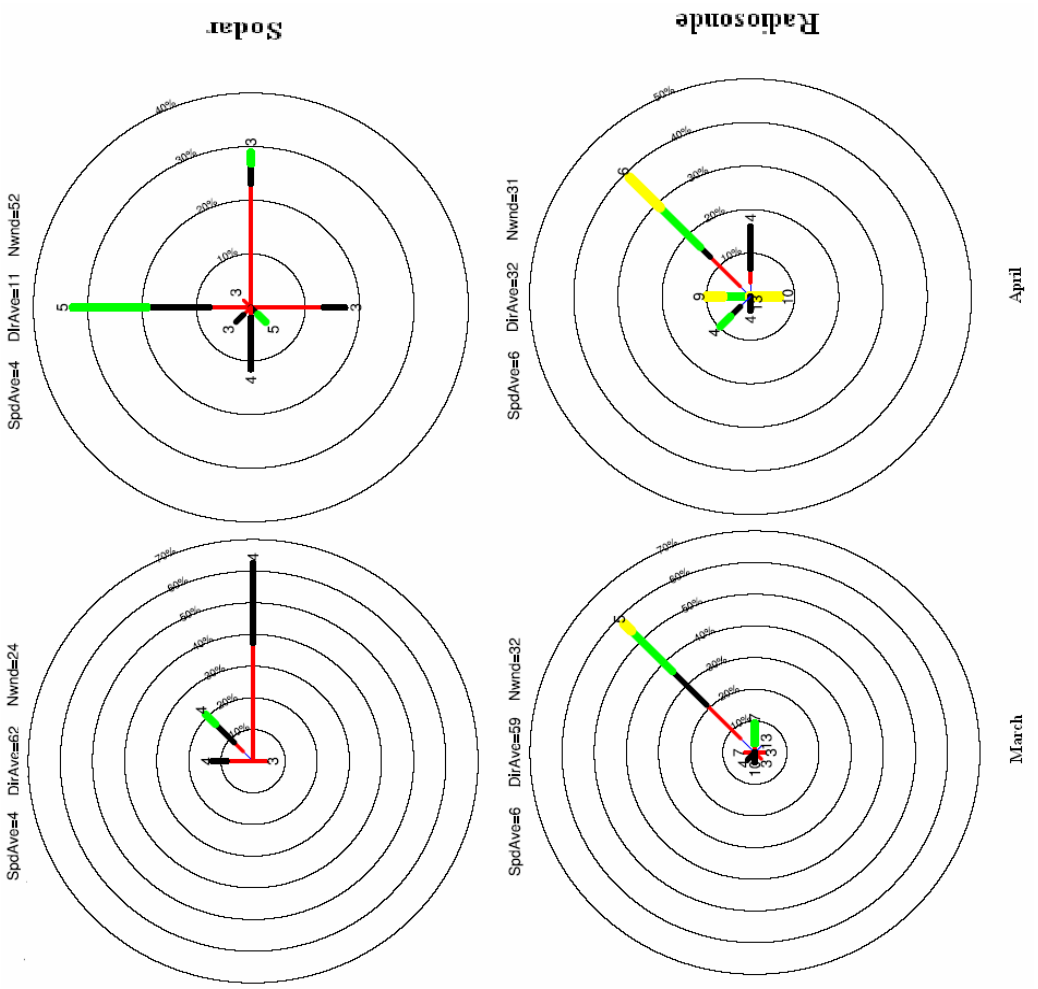

Figure 3.10 (b) Wind roses explained in Fig. 3.10 (a) for the months of March and April

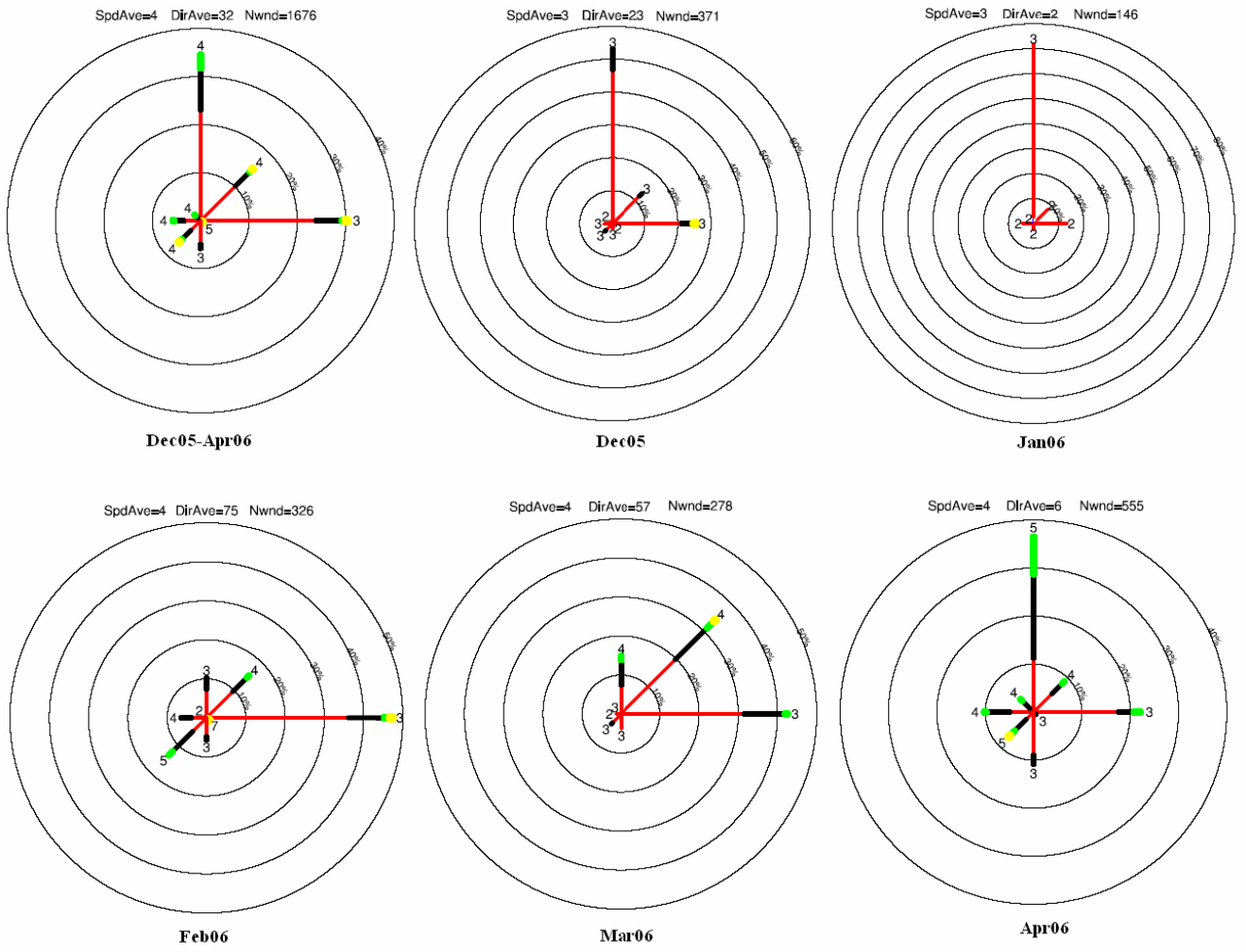

Figure 3.11 Wind roses from sodar. Wind roses from sodar observations taken at one hour intervals at an average altitude of 70m AGL.

Hartmann and Wendler (2004) investigated the change in characteristics of the surface based inversions by analyzing the twice-daily radiosonde data for December, January and February between 1957 and 2004. They plotted the frequency distribution of surface wind direction during surface inversion and no surface inversion cases for the data set as shown in Figure 3.12.

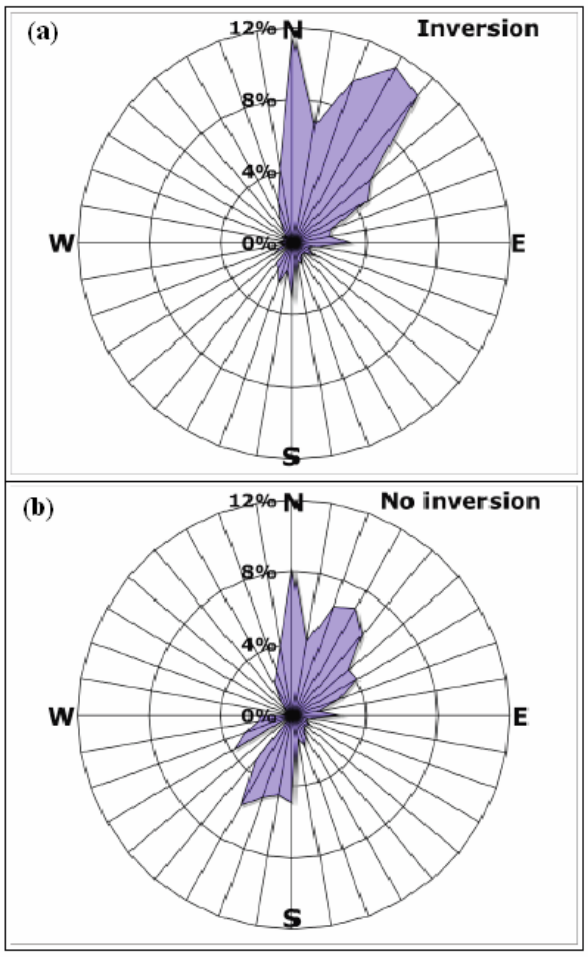

Figure 3.12 Surface wind patterns from long term radiosonde data. Frequency distribution of surface winds in December, January and February observed between 1957 and 2004 for (a) surface inversion and (b) no surface inversion cases (Source: Hartmann and Wendler, 2004)

The greater frequency of southerly winds during the 'no surface inversion' cases as seen on the bottom part of the figure is said to be a reflection of increasing frequency of warm air advection events. However a high frequency of winds from the N and the NE can be seen for the 'surface inversion' cases which on comparison with Figure 3.9 (a) shows that the wind patterns are similar in both the figures confirming that the sodar dataset from a single season is able to show the long term wind patterns observed with the radiosonde.

3.3 Case studies from sodar observations

The turbulence data that the sodar can also provide, in combination with its wind data and temperature profiles from radiosonde, can be used to study some interesting phenomena in the lower part of the atmosphere. The following discussion consists of some case studies explaining such observations from the sodar records.

3.3.1 Drainage winds overflowing the stable layer of air beneath

The main flow direction within the boundary layer in the Tanana Valley appears to be easterly or down the valley as explained in section 3.2. However, Fairbanks is surrounded by a rough semicircle of hills from the northeast to southwest and the flow pattern in this area can be extremely complex as suggested by Holmgren et al. (1975) where they show observations of two or more wind jets flowing in opposite directions in the lowest 500m from the surface. They also suggest that the surface winds may also be effectively suppressed by the combined effect of strong temperature gradient, the surrounding hills

and surface roughness elements like trees. Similar flow patterns were observed on some occasions from the wind profiles measured using the sodar. Figure 3.13 shows the profile of the wind speed and direction recorded by the sodar on December 11, 2005. The temperature profile from the two radiosonde launchings are shown at the bottom left of the figure. Also a comparison of the wind profiles recorded by the sodar and the radiosonde around the same time is presented at the bottom right of the figure. The two white vertical lines on the sodar profiles as shown in this figure and elsewhere in the thesis indicate the twice daily radiosonde launching instances.

The early morning sounding shows a strong surface based inversion up to a height of 70m above which a weaker inversion extends up to 400m. The wind profiles from the sodar show a northwesterly wind in the lower layer and an easterly wind with higher speed in the layer above. The presence of low winds within the strong inversion layer and higher winds aloft in the weaker inversion layer indicates that the easterly wind at the top may be a part of the drainage wind flowing down the Tanana Valley which overrides the stable layer of air near the ground formed due to the strong inversion. The northwesterly wind direction near the ground may be due to the drainage of cold air from the surrounding hills.

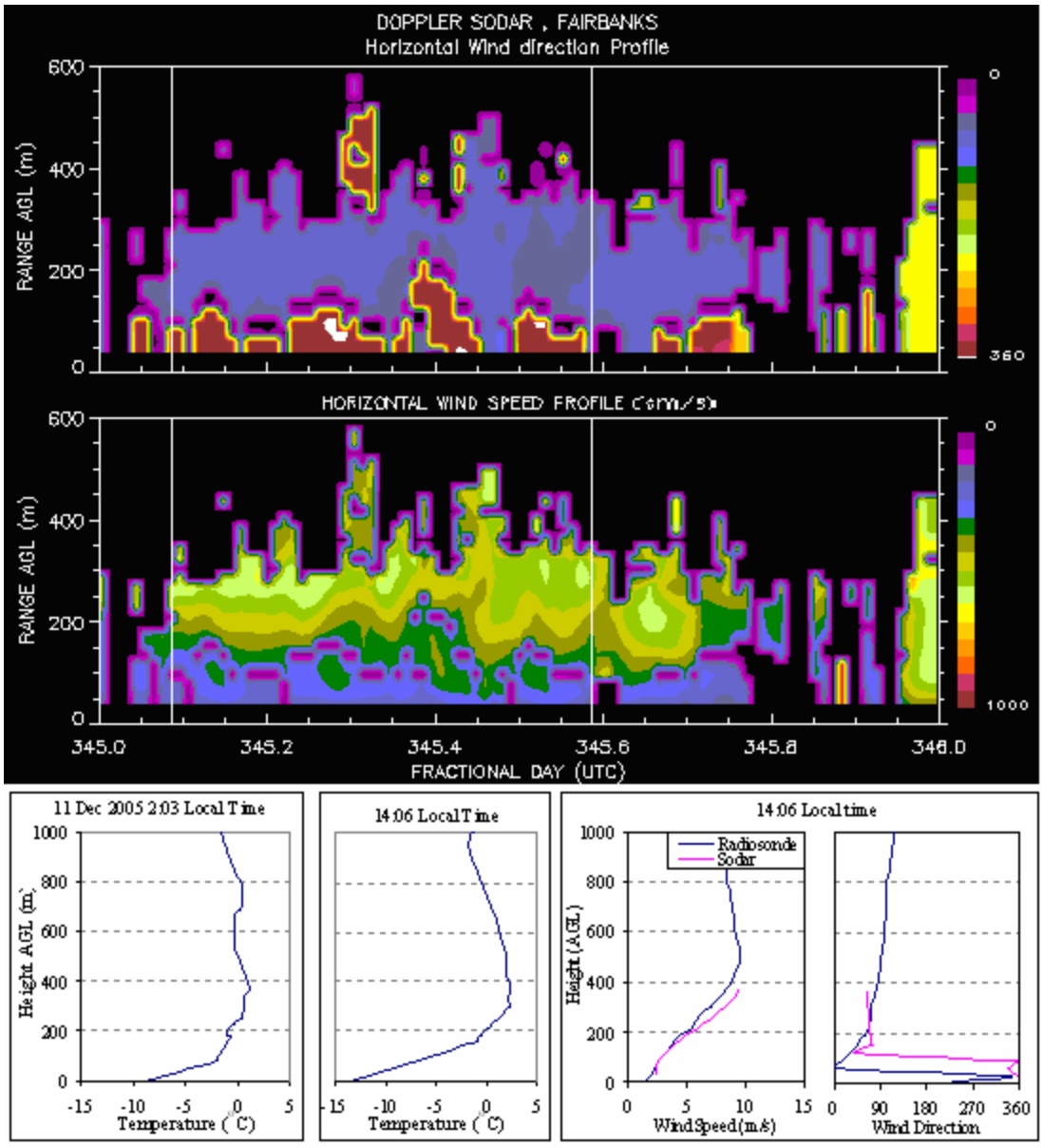

Figure 3.13 Drainage winds. (Top) Profiles of wind speed and direction recorded by the sodar on 11 December 2005 between 00:00 and 23:45. The abscissa shows the fractional Julian day and the ordinate show the height in m AGL. The wind direction is indicated on a color scale ranging from 0 to 360^{o} shown on top right and the magnitude of the wind speed is indicated on a color scale ranging from 0 to 1000 cms^{-1}. (Bottom left) Temperature profiles from the twice daily radiosonde observations. (Bottom right) Comparison of wind speed and direction profiles recorded by sodar and radiosonde.

3.3.2 Nocturnal jet associated with a temperature inversion

According to Holmgren et al. (1975) wind jets are common in Fairbanks area in situations with deep inversions. A jet is a narrow current of fast-moving air that can exist at different heights in the troposphere with variations in strength, width and length. The jets that exist much lower in the atmosphere are usually referred to as 'Low Level Jets' (LLJ) (Davies, 2000). A LLJ forms, in many cases, during the night and are often also called nocturnal jets (Stull, 1988). The nocturnal jet is an important safety factor to be considered in many aviation activities due to the vertical wind shear associated with the jet. The jets are also relevant in pollutant dispersal as the pollutants in the zone of fast moving air within the jet can be transported to great distances downwind, away from the source, even though the surface and gradient winds may remain light (Davies, 2000). Numerous mechanisms have been proposed for explaining the development mechanism of a LLJ and in some situations more than one factor contributes to the jet formation. But in the case of a nocturnal jet, considering relatively flat inland terrain and absence of synoptic-scale baroclinity associated with weather patterns, Davies (2000) using a one-dimensional model found that the jet is a result of a hybrid between an inertial oscillation in a layer within and above the jet core and a quasi-steady jet within the inversion.

The continuous and frequent recordings of wind profiles by the sodar provide an excellent chance to observe such jets. Fig 3.14 shows the sodar wind profile recorded over a 24 hour period starting from 12:00 PM local time on 29 March 2006 and extending to 12:00 PM the following day. The temperature profiles from the radiosonde soundings are shown in the middle and the bottom part of the figure shows the wind profiles at

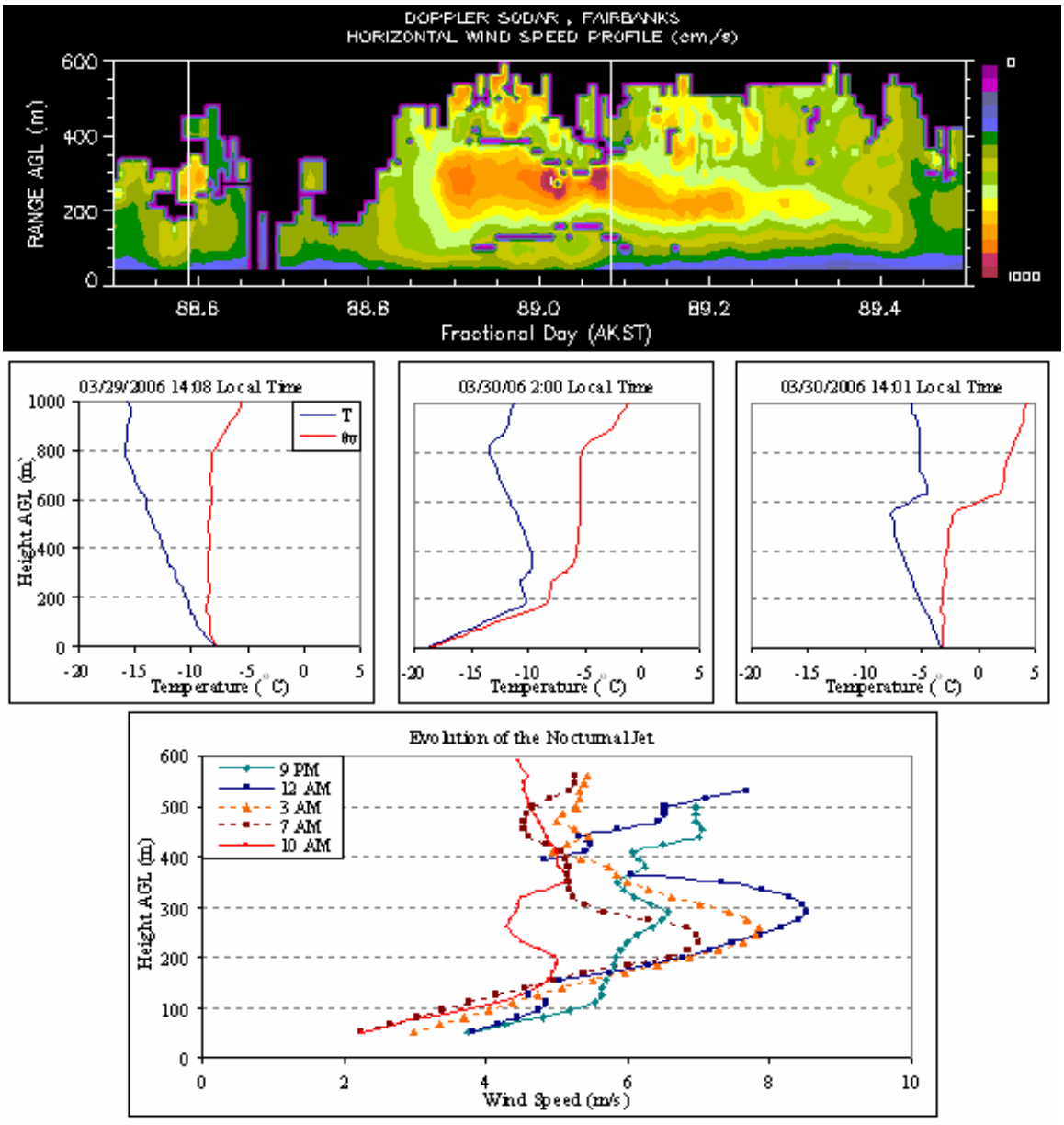

Figure 3.14 Low-level nocturnal jet. (Top) Horizontal wind speed profile from sodar data starting from 12:00 PM 29 March 2006 to 12:00 PM the following day. (Middle) Temperature profiles from radiosonde data available during the above mentioned recording period. (Bottom) Wind profiles at different intervals showing the evolution of the nocturnal jet.

different instances. The Virtual Potential Temperature (VPT) profile at 14:08 shows a mixed layer extending to a height of 800m but later in the night a surface based inversion is formed that extends up to a height of 200m. The following day the inversion is destroyed by late morning and a mixed layer is formed up to a height of 600m as evident from the VPT profile taken at 14:01. The sodar wind profile shows that around 21:00 local time a nocturnal jet starts to form near the top of the inversion. The jet lasts till the early morning and begins to fade away later in the day.

The strong frictional drag at the ground causes the winds in the ML to be subgeostrophic. When a nocturnal inversion forms at the surface, the layer above the inversion is decoupled from the surface and does not experience the frictional constraints, the pressure gradient accelerates the winds back toward geostrophic value above the inversion. According to Blackadar (1957) the Coriolis force induces an undamped inertial oscillation of the ageostrophic component of the wind, which arises from the stress divergence or friction in the daytime boundary layer, in the stress free layer above the nocturnal inversion. The period of oscillation, called the inertial period, is given by $2\pi/f_c$ where f_c is the Coriolis parameter. When the ageostrophic component is aligned with the geostrophic wind the winds at the top of the inversion become supergeostrophic. The evolution of the jet can be seen on the bottom part of Figure 3.13 showing the wind profiles at different instances. The jet generates turbulence due to the vertical wind shear associated with it and the inversion layer must be stable enough to absorb the turbulence in order to sustain the jet the same reason due to which the jet breaks down later in the morning as the inversion weakens.

3.3.3 Destruction of an inversion due to forced mixing and increasing cloud cover

A surface based inversion can be eroded in the presence of strong winds aloft due to forced mixing. Also as explained in section 3.1.2 an inversion layer can be weakened or destroyed in the presence of clouds due to a decrease in the net outgoing radiation. A lower surface pressure is often associated with stronger winds and more cloudiness and hence an inversion is often weakened or destroyed in the presence of a low pressure system. Figure 3.15 shows the surface pressure plots at different instances showing the progression of a low pressure system over Fairbanks area. The low pressure system present at the southern part of Alaska at 3:00 Local Time on 12 February 2006 (denoted by an L with the number 988) moves over Fairbanks and weakens (now 995 mb) by 15:00 local time the same day. It continues moving to the north and rapidly dissipates. The following day, 13 February, a high pressure ridge builds over Fairbanks and by 21:00 local time is well established, causing clear sky conditions. The sodar observations during this time period are explained in the following discussion.

Figure 3.16 shows the profiles of winds and C_T^2 recorded by the sodar over a period of three days beginning from 00:00 Local time on 12 February 2006 and ending at 23:30 local time on 14 February 2006. The bottom part of the figure shows the temperature profiles from the twice daily radiosonde observations taken during these three days. The temperature profiles show a strong surface based inversion on 12 February which is destroyed by the following day. The inversion has re-formed by the early morning of 14 February. An examination of the sodar wind profiles shows that around 3:30 Local time on 12 February, when the low pressure system is over Fairbanks, the wind direction

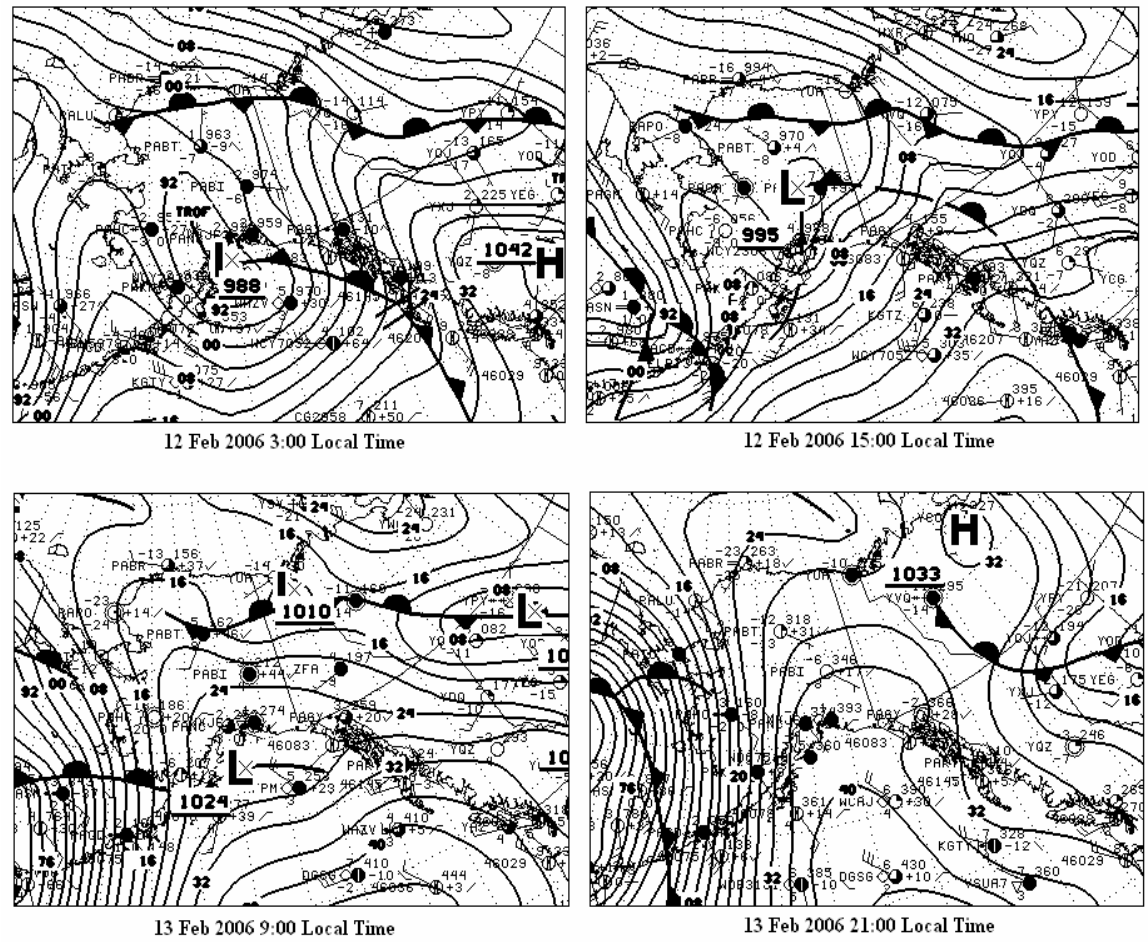

Figure 3.15 Low pressure system over Fairbanks area. Surface pressure plots at different instances showing the progression of a low pressure system over Fairbanks area.

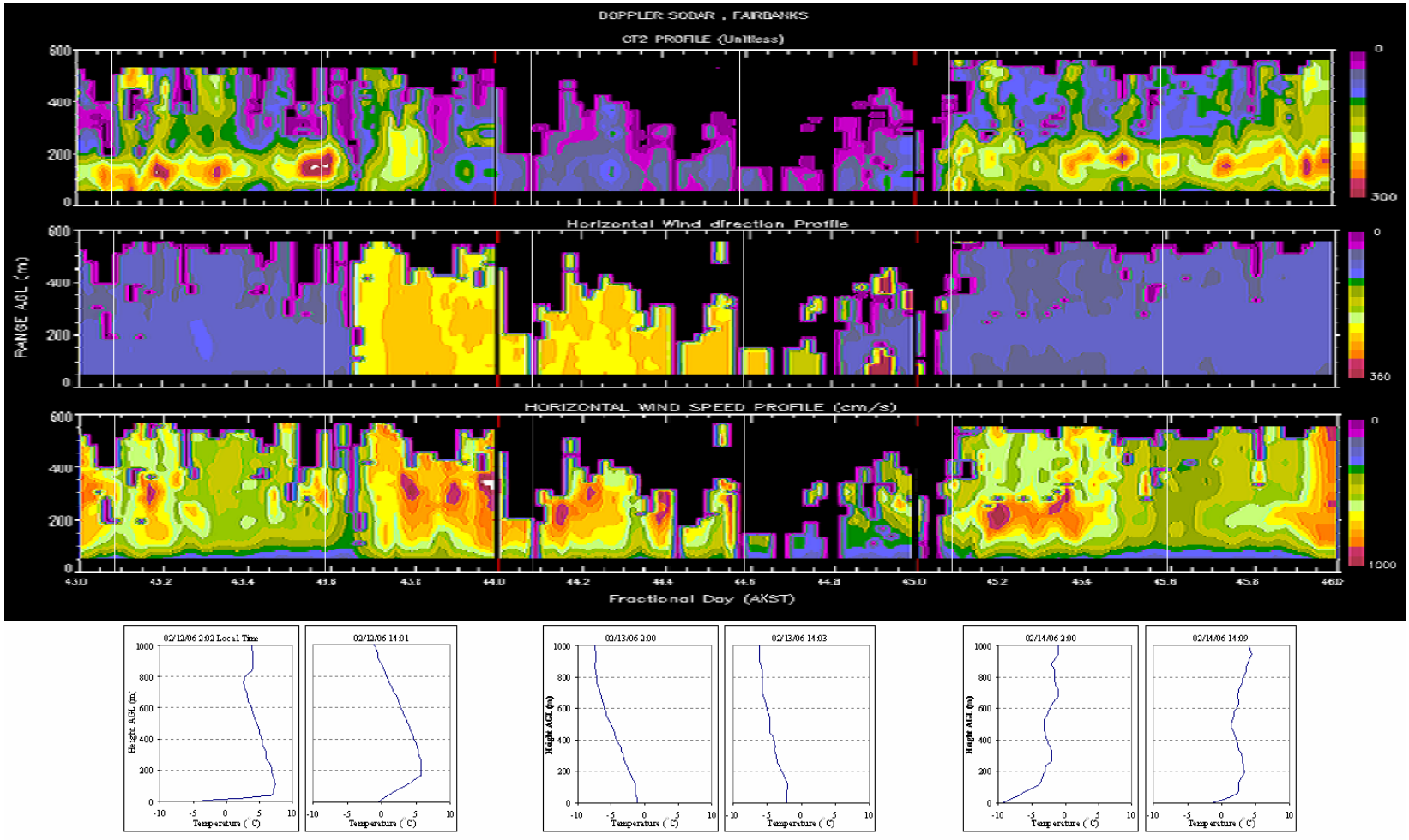

Figure 3.16 Destruction and formation of temperature inversion. (Top) Profiles of C_T^2, wind direction and speed recorded by sodar from 00:00 on 12 February 2006 to 23: 30 on 14 Febbruary 2006. The red lines on the abscissa indicate the end of each day and the white vertical lines on the profiles indicate the radiosonde launching instants. (Bottom) Temperature profiles from the twice daily radiosonde launches during the time period shown in the sodar profiles

changes from easterly to southwesterly and the wind speed also increases. The low pressure system results in cloudy conditions and causes advection of warmer and moister air from the south with higher wind speeds. Due to this the surface based inversion is destroyed through cloud radiative effects and forced mixing. The destruction of the inversion can be clearly seen on the C_T^2 profile from the sodar on 12 February. The higher value of C_T^2 up to 200m is due the thermal fluctuations within the inversion layer. This band of higher C_T^2 fades away at the point when the wind direction changes indicating the destruction of inversion. Following the dissipation of the low pressure system a high pressure ridge is formed on the night of 13 February causing clear sky conditions and low wind speeds allowing the inversion to re-form. Again the C_T^2 profile clearly shows the formation and persistence of the inversion on 14 February.

3.3.4 Estimation of mixing layer height from the backscatter intensity

The structure of the Atmospheric Boundary Layer (ABL) strongly determines the dispersion and transport of the trace gases and pollutants in the lower atmosphere. The height of the Mixing Layer (ML) is an important parameter in predicting the evolution of the ABL and its diffusion capabilities and hence real-time information on the ML height is valuable for a wide range of meteorological and air pollution applications.

The Mixing Layer is characterized by well developed turbulence which tends to mix heat, moisture and momentum uniformly in the vertical. The turbulence in the mixed layer is usually convectively driven by maintenance of an unstable profile due to solar heating of the surface and radiative cooling at the top of the cloud layer. Due to the

surface heating, a shallow convective layer is formed after sunrise underneath the nighttime created stable inversion. Thermals of warm air rise from the ground and the convective layer grows by entraining the less turbulent air from above. The mixing layer reaches its maximum height in late afternoon. The capping inversion at the top of the ML acts as a lid to the rising thermals. The height of the inversion base is usually regarded as the ML height.

The ML height estimation in most cases is based on profile data of mean meteorological variables from standard radiosonde ascents but during the last two decades, sodar data have been increasingly used to estimate the height of the ML (Beyrich et al., 1996). The spatial average of the determined atmospheric parameters by the acoustic sounding system is often more appropriate than single point measurements in studies of the ABL (Asimakopoulos et al., 2004). The temperature inversion layers in general are associated with a higher intensity of the backscattered acoustic signal. Thus the Mixing layer height can be determined by identifying the base of the capping inversion from the visual inspection of the backscattered acoustic intensity profile.

The following discussion is an ideal illustration of a case where the ML height can be unambiguously determined from the sodar data using the procedure described above. Figure 3.17 shows the profile of the C_T^2 value, proportional to the backscattered power, recorded by the sodar on April 24, 2006 for the entire 24 hours with an averaging time of 15 minutes. The temperature and the mixing ratio profiles from the two radiosonde launches are shown at the bottom of the figure. At 3:04 Local Time an inversion layer extending up to 200m from the surface can be observed from the temperature profile. The

presence of this layer is also reflected in the C_T^2 profile from the sodar which shows higher values up to a height of 200m early in the morning. The higher C_T^2 values within the inversion layer are due to the great amount of energy backscattered due to the thermal fluctuations within the layer. However the C_T^2 profile during the late afternoon shows a second maximum in the profile from 350m and above. The wind speeds recorded by the sodar show no strong wind shears at that region. Thus, as described in Soler et al. (1996),

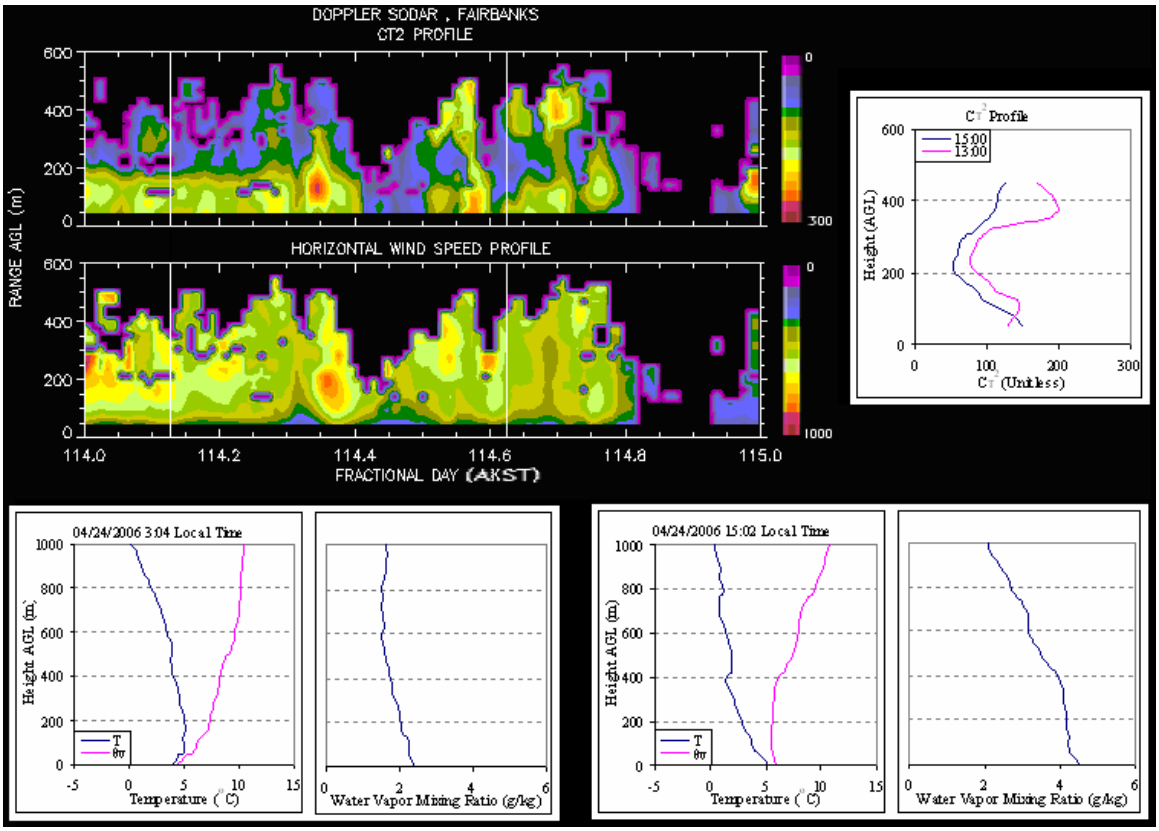

Figure 3.17 Mixing layer height. (Top Left) Profiles of C_T^2 and wind speed recorded by sodar on 24 April 2006 from 00:00 to 23:45 local time. The magnitude of the quantities in indicated on a color scale shown on the right side of each profile. (Top Right) C_T^2 profiles shown separately for two instants. (Bottom) Profiles of temperature, virtual potential temperature and water vapor mixing ratio from the radiosonde data.

it can be inferred that the second maximum in C_T^2 occurs due to the presence of the capping inversion at the top of the ML while the higher C_T^2 values near the surface are due to the presence of convection. The right side of the figure shows the same C_T^2 profile, given at the end of the averaging period, at two different instants. It shows that the elevated maximum in C_T^2 is at a height of 380m which suggests that ML is 380m deep. The temperature profile from the radiosonde data at 15:02 shows an elevated inversion at this altitude while the VPT and mixing ratio are fairly constant up to the base of the elevated inversion thus confirming the presence of a well mixed layer below the capping inversion.

Chapter 4 Conclusions and future work

The winter time temperature inversions in Fairbanks, Alaska are among the strongest in the world due to its high latitude, distance from the sea and sheltered location, which also causes low wind speeds near the surface. Although Fairbanks is a comparatively small city, the per capita energy consumption is very high giving rise to pollutants, moisture and waste heat. During these situations of extreme ground inversions and low wind speeds a turbulent mixing layer, characterized by well-developed turbulence and approximately height-independent fluxes of heat and momentum, is generally missing at the surface. As a result, surface pollutants such as combustion products and ice fog, when the temperature decreases below about -38°C, are trapped generally within a few hundred feet above the ground causing serious air pollution episodes in this area.

Previous research work shows a strong connection between the occurrence of lowest temperatures in Fairbanks with high pressure systems and clear skies, situations in which a sharp temperature drop at the surface is observed and a surface inversion is built up. During winter the wind speeds in Fairbanks are very low, a condition that assists in maintaining the strong inversions, and both speed and direction are strongly controlled by the topography with stronger winds generated on steep slopes and weaker winds on relatively flat terrain. The main flow direction within the boundary layer in the Tanana Valley is usually easterly, or down the Valley, but is more complex in Fairbanks. A northerly or northwesterly wind direction, or calm, is associated with the strongest

inversions, which is due to the gravity wind drainage from the surrounding hills under stable conditions.

A continuous measurement of winds and turbulence is desirable for a better understanding of the structure of the lower atmosphere and its variations. The sodar or acoustic sounder is proved to be a very useful instrument for studying the lower atmosphere as it can continuously and reliably measure the vertical profiles of wind speed and direction, vertical motions, turbulence and the thermal structure in the lower part of the troposphere. The direct and strong interaction of sound waves with the microstructure of the atmosphere, the low cost of antennas and the ease of installation are the factors that make the sodars unique instruments for studying the lower atmosphere.

Based on this idea a commercially available Doppler sodar was installed at the NWS site in Fairbanks and was successfully operated on a continuous basis from December 2005 to April 2006. The low turbulent conditions in the winter months limited the maximum altitude of the available data to less than what was anticipated. Though the data availability was intermittent, as some of the transducers in the phased array antenna were not functional at times due to the severely cold conditions, enough data could be acquired to perform a useful analysis.

As an auxiliary to the Doppler sodar measurements, a simple algorithm was developed to identify strong layers of temperature inversions from the high resolution radiosonde data. The analysis of the results from the algorithm showed that the algorithm successfully captured the trends in the characteristics of inversions. The inversions were stronger, deeper and more frequent during the coldest months of December and January

with most of them being surface based during both day and nighttime. The diurnal variation in surface temperatures and the characteristics of inversions were more pronounced for the warmer months of March and April due to the increasing amount of solar radiation available during the daytime. Also there was an increased frequency of elevated inversions, during both day and night, progressing towards the warmer months and most of the daytime inversions were elevated during March and April. The characteristics of inversions were also investigated based on the sky cloud cover. Beginning from early spring the inversions during the nights are found to be much stronger than the corresponding daytime inversions during clear sky conditions with most of the inversions being surface based during day and night even in the relatively warmer months. However on cloudy nights a majority of inversion layers are elevated in the warmer months with some elevated layers found even during the colder winter months.

The winter/spring wind data from the sodar indicated that the majority of winds close to the surface in Fairbanks area are from the N, NE or E which is due to the large scale air drainage down the Tanana Valley and from the surrounding hills under strong inversion conditions. The frequency of the winds from the other directions increased progressing towards the warmer months as the inversions become weaker and less frequent. A comparison of the sodar wind data with the concurrent radiosonde data showed a good agreement. However the sodar underestimated the wind speeds by 2 ms^{-1} which might be due to the averaging involved in the sodar measurements. The sodar wind observations also compared well with the long term wind patterns over the Fairbanks area. The ability of the sodar to provide continuous observations of winds and turbulence

data was valuable in carrying out case studies depicting drainage winds, low-level nocturnal jets, break up and formation of inversions and the estimating the mixing layer height.

Future studies if carried out with an ability to access the single shot data along with the processed data would be valuable in understanding other phenomenon like gravity waves and multiple layers of inversions as observed in previous research work in Fairbanks. Also, it would be beneficial to better equip the sodar for the severely cold conditions in such locations.

References

Asimakopoulos, D.N., C.G. Helmis, and J. Michopoulos, 2004: Evaluation of SODAR methods for the determination of the atmospheric boundary layer mixing height. *Meteorology and Atmospheric Physics, Vol. 85, 85-92.*

Batchelor, G.K., 1957: Wave scattering due to turbulence. *Symposium on Naval Hydrodynamics (F.S. Sherman, Ed.), NASNRC Publication No. 515, National Research Council, Washington, D.C., 409-430.*

Benson, C.S., 1970: Ice Fog: Low temperature air pollution. *Cold Regions Research Engineering Laboratory, Hanover, N.H. Research Report 121.*

Benson, C.S., and G.E. Weller, 1969: A study of low-level winds in the vicinity of Fairbanks, Alaska. *Report to Earth resources Company, Geophysical Institute, University of Alaska, Fairbanks.*

Benson, C.S., S.A. Bowling, and G.E. Weller, 1983: Urban climates in Alaska. *Environments 15, 23-36.*

Beyrich, F., U. Weisensee, D. Sprung, and H. Gusten, 1996: Comparative analysis of Sodar and ozone profile measurements in a complex structured boundary layer and implications for mixing height estimation. *Boundary-Layer Meteorology 81, 1-9.*

Bilello, M.A., 1966: Survey of arctic and subarctic temperature inversions. *CRREL Technical Report, 161.*

Blackadar, A.K., 1957: Boundary layer maxima and their significance for the growth of nocturnal inversions. *Bulletin of American Meteorological Society, 38, 283-290.*

Bowling, S., T. Ohtake, and C.S. Benson, 1968: Winter pressure systems and ice fog in Fairbanks, Alaska. *Journal of Applied Meteorology, 7, No. 6, 961-968.*

Bowling, S.A., and C.S. Benson, 1978: Study of the Subarctic Heat Island at Fairbanks, Alaska. *Environmental Protection Agency Report EPA-600/4-78-027, 150 pp.*

Davies, P.A., 2000: Development and mechanisms of the nocturnal jet. *Meteorological Applications, Vol. 7, 239-246.*

EPA QA Handbook of air pollution measurement systems, Vol. 4. *Meteorological Measurements, Version 1.0*

Gsonik, T.A., and C.S. Benson, 1982: Aspects of Far-Northern Air pollution with particular reference to Fairbanks, Alaska. *Geophysical Institute Report UAG R-291, University of Alaska, 34 pp.*

Hartmann, B., and G. Wendler, 2004: Climatology of the winter surface temperature inversion in Fairbanks, Alaska. *Conference on Polar Meteorology and Oceanography, Vol. 8.*

Holmgren, B., L. Spears, C. Wilson, and C.S. Benson, 1975: Acoustic Soundings of the Fairbanks Temperature Inversions. *Climate of the Arctic, Geophysical Institute, University of Alaska, 293-306.*

Holty, J.G., 1973: Air Quality in a Subarctic Community, Fairbanks, Alaska. *Arctic, 26, 292-302.*

Jayaweera, K., Wendler, G., and T. Ohtake, 1975: Low Cloud Cover and the Winter Temperature of Fairbanks. *Climate of the Arctic: Proceedings, 316-322.*

Kahl, J.D., 1990: Characteristics of the Low-Level Temperature Inversion along the Alaskan arctic coast. *International Journal of Climatology, Vol. 10, 537-548.*

Landsberg, H.E., 1981: The Urban Climate. *International Geophysics Series, Vol. 28, 275 pp., Academic, San Diego, California.*

Liou, K.N., 2002: An Introduction to Atmospheric Radiation, Second Edition. *International Geophysics Series, Vol. 84. Academic Press.*

Little, C.G., 1969: Acoustic methods for the remote probing of the lower atmosphere. *Proceedings IEEE, 57, 571-578.*

Marvill, S., and K. Jayaweera, 1975: Investigations of Strong Valley Winds in Alaska using Satellite Infrared Imagery. *Monthly Weather Review, Vol. 103, No. 12, 1129-1136.*

McAllister, L.G., 1969: Acoustic sounding of lower troposphere. *Journal of Atmospheric and Terrestrial Physics, 30, 1439-1440.*

Neff, W.D., and R.L. Coulter, 1986: Acoustic Remote Sensing. *Probing the Atmospheric Boundary Layer, D.H. Lenschow (Ed.), American Meteorological Society, Boston. 201-239.*

Soler, M.R., J. Hinojosa, and J. Cuxart, 1996: Atmospheric thermic structure studied by acoustic echo sounder, Boundary layer model, and direct measurements. *Boundary-Layer Meteorology 81, 35-47.*

Stull, R.B., 1988: An Introduction of Boundary Layer Meteorology. *Atmospheric and Oceanographic Sciences Library, Kluwer Academic Publishers, Vol. 13, 680 pp.*

Tatarskii, V. I., 1971: The Effects of the Turbulent Atmosphere on Wave Propagation. *Israel Program for Scientific Translations, 471 pp.*

The Ongoing Challenge of Managing Carbon Monoxide Pollution in Fairbanks, Alaska. *Committee on Carbon Monoxide Episodes in Meteorological and Topographical Problem Areas, National Research Council, 2002.*

Wendler, G.D., 1969: Heat balance studies during an ice-fog period in Fairbanks, Alaska. *Monthly Weather Review, Vol. 97, 512-520.*

Wendler, G., and P. Nicpon, 1975: Low-Level Temperature Inversions in Fairbanks, Central Alaska. *Monthly Weather Review, Vol. 103, No. 1, 34-44.*

Winchester, J.W., W.H. Zoller, R.A. Duce, and C.S. Benson, 1967: Lead and Halogens in Pollution Aerosols and Snow from Fairbanks, Alaska. *Atmospheric Environment, Vol. 1, 105-119.*